

Article

## Development of a Model for Charge Transport in Conjugated Polymers

Xuezheng Wang, Benjamin Shapiro, and Elisabeth Smela

*J. Phys. Chem. C*, **2009**, 113 (1), 382-401 • Publication Date (Web): 11 December 2008

Downloaded from <http://pubs.acs.org> on January 12, 2009

### More About This Article

---

Additional resources and features associated with this article are available within the HTML version:

- Supporting Information
- Access to high resolution figures
- Links to articles and content related to this article
- Copyright permission to reproduce figures and/or text from this article

[View the Full Text HTML](#)

## Development of a Model for Charge Transport in Conjugated Polymers

Xuezheng Wang,<sup>†</sup> Benjamin Shapiro,<sup>‡</sup> and Elisabeth Smela<sup>\*,†</sup>

Department of Mechanical Engineering, University of Maryland, College Park, Maryland 20742, and  
Department of Aerospace Engineering, University of Maryland, College Park, Maryland 20742

Received: April 4, 2008; Revised Manuscript Received: October 1, 2008

A finite element model for charge transport in conjugated polymers is developed based on transport equations for ionic and electronic charge coupled with the Poisson equation. The model behavior is fully explored, and its complexity is gradually increased to realize a full model that treats non-Fickian diffusion through nonconstant coefficients and that includes ion transport in the electrolyte. The simulation results are compared qualitatively with the experimental results for an ion-barrier-covered PPy(DBS) film during electrochemical reduction, and the model is found to successfully account for the dominant behaviors, including the emergence of a front. One of the key findings of the simulations is that migration must be taken into account to correctly describe ion ingress: none of the various simulations in which ion transport was only by diffusion predicted the experimental results. Another is that the front velocity is proportional to the applied voltage, as found experimentally, and that the cation front can move into the polymer with a velocity  $v \sim \sqrt{t}$  even when the ions move by migration alone.

### 1. Introduction

Ion and hole transport occur in those applications of conjugated polymers in which the device operation depends on significant changes in the oxidation level of the polymer, including batteries and supercapacitors, electrochromic displays, actuators, and chemical sensors. It is therefore important to understand what governs the movements of these charged particles in response to an applied voltage in a system in which their local concentrations, as well as the electrical conductivities and other properties of the materials through which they move, are changing over time.

The goal of the work in this paper was to develop a general model based on fundamental equations that would account for the dominant features of charge transport in conjugated polymers during electrochemical switching between fully oxidized and reduced states. Such a model should ideally have no adjustable parameters and should account for the main effects, if not all the details. Such modeling based on first principles is not the same as curve-fitting. The model presented here is also not a black-box model, such as a lumped parameter equivalent circuit model, although such models have been successfully applied to some aspects of switching behavior (see, for example, refs 1 and 2).

The model is focused on ion transport in/out and through the polymer since ion ingress is the primary contributor to volume expansion in actuators and since ion transport is often the rate-limiting step during electrochemical switching. Because it is aimed at predicting device performance, the model is phrased on a length scale that is small compared with the device but large enough to allow the use of a continuum assumption (see section 3.1.1), which makes modeling by partial differential equations possible. The model includes ion transport (in the polymer and also, for the full model, in the electrolyte), hole transport (polarons, bipolarons), and the electric fields that drive

transport (both those that are applied to the material and those generated by the charges themselves). The equations used during the initial stages of model development are standard, but their simulation is not. Simulation of charge transport in these materials has not been done previously, and the details of how this was done were critical to its success. This paper thus goes into sufficient detail to enable others to reproduce this work. In the later parts of this paper, the transport equations are modified to make the coefficients concentration-dependent, and those equations are not standard.

The model does not yet explicitly include the effects of changes in the packing of the polymer matrix (electrochemically stimulated conformational relaxation, ESCR, effects) or the electrochemical reactions themselves (it examines only switching between the fully oxidized and fully reduced states, assuming that hole transfer between the electrodes is energetically allowed and fast). In other words, the chemical nature of the process and the polymeric nature of the material are ignored in this initial physical approach, even though under some experimental conditions the chemical reactions and the conformational movements of the chains can be the rate-limiting steps. Including these effects in the initial model would be premature and so must be reserved for future work. That is not to say that these effects are not critical, but that building a too-complex, all-encompassing model from the beginning does not allow one to gain a sufficiently thorough understanding of the reasons for the model's behavior to enable confidence in its predictions. ESCR effects are already well-modeled, and joining this new model with that one would be a next logical step.

Model development was informed only by the behaviors observed during reduction of an ion-barrier-covered film of PPy(DBS).<sup>3,4</sup> If the basic physics of the charge transport is properly captured by the model, then it should correctly predict what happens under other conditions, such as reversing the voltage to reoxidize the polymer. This will be done in future papers.

This modeling work expands upon that done by Lacroix et al.,<sup>5</sup> who modeled the movement of electrons and ions in

\* Corresponding author. Tel.: 301-405-5265. Fax: 301-314-9477. E-mail: smela@eng.umd.edu.

<sup>†</sup> Department of Mechanical Engineering.

<sup>‡</sup> Department of Aerospace Engineering.

conjugated polymers, examining several limiting cases *analytically*. Here, we take the same basic equations governing electron and ion movements, allow their coefficients to be functions of state (to, for example, try to capture non-Fickian diffusion), subject them to boundary conditions, and *simulate* them, allowing us to examine virtually any case of interest. Simulations offer the advantage of allowing one to visualize the charge concentrations, electric fields, and other variables as they evolve over time. By simulating the geometry described in refs 3 and 4, we are able to qualitatively compare the results of the simulations with the experimental results.

Other prior modeling based on first principles has been done with the aim of predicting the shape of cyclic voltammograms. Those models used simplifying assumptions to make the problem tractable, such as that ions moved solely by ordinary diffusion, that changes in the number of charges on the backbone did not need to be considered, or that charge neutrality held everywhere.<sup>6–8</sup> The current model does not make these assumptions and thus advances that prior work. However, as mentioned above, in this paper we do not consider the energetics or kinetics of electron transfer between the polymer and the electrode (i.e., the electrochemistry) and only examine switching to potentials at which this transfer is possible and fast. Including the information on polymer energy levels contained in cyclic voltammograms is outside the scope of this work but should also be included in future, more sophisticated models.

The main contribution of this paper to our understanding of oxidation/reduction (redox) in conjugated polymers is a fully characterized, physics-based model whose parameters were chosen by taking values from the literature. There was no tweaking of parameters to match experimental behavior. Such first-principles modeling is needed to understand device behavior and to design alternative behaviors. Our simulation code is available upon request (a license for the commercial software package FEMLAB/COMSOL (Comsol AB, www.comsol.com) will be required to run the code).

One of the most important conclusions of this paper is that no scenario in which the ions move in the polymer solely by diffusion correctly accounts for the experimental results seen in ref 4; it is necessary to include migration for the model to reproduce the experimental ion profiles. A second conclusion is that this model, despite the fact that it leaves out electrochemical and polymeric contributions, achieves the goal of explaining the dominant behaviors seen during electrochemical reduction (without adjustable parameters).

The paper is organized as follows. (*The reader who is not interested in modeling details may wish to skip directly to the results in section 5.*) First, a broad overview of the model is given in section 2. The modeling methods are detailed in section 3: the assumptions, governing equations, boundary conditions, etc. Section 4 explores the behavior of a bare-bones “base case” model. This case is necessary to understand the basic behavior of the model. Simulations are run to verify that the model gives reasonable results, and the effect of varying the model parameters is examined. This yields a qualitative understanding of the roles of the material constants and boundary conditions. In section 5, the complexity of the model is increased to better reflect the physical system, resulting in a “full model”. Modeling cases that address some of the phenomena observed experimentally—such as nonconstant mobilities and non-Fickian diffusion—as well as cases that address open questions in the literature—such as whether charge neutrality is strictly enforced in the material—are treated here. Section 6 summarizes all the model development results, and section 7 ends with a summary and conclusions.

## 2. Model Overview

In this section, we summarize the effects that are included in the model and why, based on our understanding of the physical system. The three partial differential equations (PDEs) of the model are introduced, and terms are defined.

The model presented here explicitly accounts for the movement of both ionic charge and electronic charge (polarons and bipolarons on the polymer backbone, referred to herein as “holes” in analogy to the positive charges in inorganic semiconductors). In prior versions of this model, hole transport was either neglected<sup>9</sup> or the assumption was made, based on experimental estimates in the literature of the relative mobilities of the polarons and the ions, that the holes move instantaneously relative to the ions.<sup>10</sup> The latter approach allowed us to formulate an analytical solution for the hole transport. This simplifying assumption has been lifted here.

There are three mechanisms for charge transport: diffusion, drift (also called migration), and convection. Diffusion occurs in the presence of concentration gradients. Fickian diffusion arises when the probabilities for particle movement are equal in all directions, i.e., if the medium is isotropic. (However, since the properties of these polymers are not isotropic during redox (see ref 4, Figure 2), diffusion cannot be Fickian.) Migration is the movement of a particle under a force, such as the movement of a charged particle under an applied voltage. As reviewed by Lacroix,<sup>5</sup> the existence of electric fields in the polymer, particularly in the reduced regions, must be taken into account. Since both ions and holes are charged species, one cannot a priori neglect their movement in electrical fields nor their electrostatic interactions. Electrochemists have traditionally combined drift and diffusion in the electrochemical potential.<sup>11</sup> For transparency, they are kept separate here. Lastly, convection is the movement of a particle carried in the flow of a fluid, like a boat in a current. This last mechanism is neglected in our model. For ion transport, it is neglected because there are no significant fluid flows through the conjugated polymer (although solvent diffuses into the polymer independently of ion transport,<sup>12</sup> this occurs at a slower time scale and does not carry ions). For hole transport, it is neglected because the polymer chains do not flow as a liquid does (although the chains do undergo local movements such as changes in conformation). In the electrolyte, convection is also neglected since the solution is unstirred. Thus, the model includes one partial differential equation (PDE) for the ion current due to drift and diffusion and a second PDE for hole drift and diffusion.

The electric fields under which the charges move arise from two sources. Physically, fields are produced by applied voltages on the electrodes and by local imbalances between the concentrations of positively and negatively charged species. It only takes a tiny charge imbalance to create a large electric field, which means that even if charge neutrality is satisfied almost everywhere net charge can still become the dominant driver for ion transport.<sup>5</sup> In the model, boundary conditions are used to specify the potentials at key interfaces, and Poisson's equation, a third PDE, relates the gradient of the electrical field inside the polymer to the net charge.

The three PDEs are coupled because the concentrations of holes and ions in the polymer depend on each other (net charge results in electric fields, which leads to charge migration). In a cation-transporting polymer like PPy(DBS), as holes are withdrawn at the electrode, charge compensating cations enter from the electrolyte. The negatively charged DBS<sup>−</sup> counterions (anions *A*) are immobile in the polymer and are treated as a fixed background in the model. The concentrations of holes *H*

and cations  $C$  sum to the concentration of anions almost everywhere, and where they do not, charge neutrality is violated and electrical fields are produced that result in charge migration.

The equations used in our work are similar to the standard ones for describing charge transport in crystalline inorganic semiconductors like silicon<sup>13</sup> and therefore may be too simple to account for all the physics occurring in the conjugated polymer during redox, a process that has no inorganic analog. However, they provide a first approximation, a starting point in the model-building process. We show in this paper that they do, in fact, account for much of the behavior seen experimentally.

Since the equations are coupled and since they have nonlinear parameter dependencies, they cannot be solved analytically for any general case. Thus, they are solved numerically using finite element modeling. After solving for the initial conditions (the polymer is either fully oxidized or fully reduced before a switching potential is applied at the boundaries), the ion, hole, and potential profiles are allowed to evolve in response to each other, simulating the redox process.

Model development was informed only by experimental results obtained during electrochemical reduction of an ion-barrier covered film of PPy(DBS). Comparison between simulation and experimental results guided the choice of initial and boundary conditions, meshing and other details of the simulation mechanics, and choices such as how to stipulate the maximum concentration of ions in the material. In later papers, we shall run the model “backwards” by reversing the voltages at the boundaries to simulate oxidation and shall modify the third PDE to reflect anion transport to simulate redox in materials such as PPy(ClO<sub>4</sub>).

### 3. Modeling Methods

This section contains the information required to reproduce the work in the remainder of this paper, as well as in subsequent papers that will utilize this model. Readers who are not interested in the internal workings of the model should skip to section 5.2.2. The assumptions going into the model and a justification of the continuum treatment are given. We describe how the model is derived and discuss the physics that were included. The governing equations are presented, as are the boundary conditions. Methods for reducing model complexity are described, as is the way the nondimensionalization was performed. Finally, the numerical methods are described, i.e., how the resulting equations were actually solved numerically.

**3.1. Model Properties. 3.1.1. Continuum Treatment.** The finite element model volume elements are 10 nm on each side. This is small compared to device length scales but large compared to polaron length scales, so it is appropriate to use a continuum assumption. Within each volume element, there are many ions and/or holes (there are  $\sim 10^3$  holes in a volume element), so that it is appropriate to consider concentrations of species instead of tracking individual molecules. (This estimate came from the following. To deposit a film 1  $\mu\text{m}$  thick consumes 200  $\text{mC}/\text{cm}^2$ ,<sup>14</sup> approximately 10% of which is used for the creation of charge carriers:  $[0.1 \times 200 \times 10^{-3} \text{ C}/(\text{cm}^2 \cdot \text{mm})]/(10^6 \times 10^6 \times 10^2)/1.6 \times 10^{-19} \text{ C}/\text{electron} \approx 1000 \text{ electrons}/(10 \text{ nm})^3$ .)

**3.1.2. Physics and Equations. 3.1.2.1. Governing Equations.** The first modeling equation (the continuity equation<sup>15</sup>) expresses the conservation of species

$$\frac{\partial C_i}{\partial t} = -\nabla \cdot \vec{J}_i \quad (1)$$

where  $C_i$  is the concentration of species  $i$  ( $\text{mol}/\text{cm}^3$ ) and  $\vec{J}_i$  is the flux ( $\text{mol}/\text{s cm}^2$ ).  $C_i$  is a dynamic variable that depends on

space and time, so  $C_i = C_i(x, y, z, t)$ . This equation has no source/sink terms and thus holds in the absence of species generation (e.g., by light) or annihilation.

The flux  $\vec{J}_i$  must be expressed in terms of the physical conditions. As mentioned previously, we ignore convection but consider diffusion and drift,  $\vec{J}_i = \vec{J}_i^{\text{diff}} + \vec{J}_i^{\text{drift}}$ . Commonly used models for each of these components in inorganic semiconductors are<sup>11,13</sup>

$$\vec{J}_i^{\text{diff}} = -D_i \nabla C_i \quad (2)$$

where  $D_i$  is the diffusion coefficient ( $\text{cm}^2/\text{s}$ ) and

$$\vec{J}_i^{\text{drift}} = z_i \mu_i C_i \vec{E} \quad (3)$$

where  $z_i$  is the positive or negative charge per species molecule;  $\mu_i$  is the mobility ( $\text{cm}^2/\text{V s}$ ); and  $\vec{E}$  is the electric field, and where  $\vec{E} = -\nabla\phi$  and  $\phi$  is the electric potential. (There are of course other ways of formulating the currents, involving, e.g., quasichemical potentials,<sup>16</sup> particle jump probabilities in different directions,<sup>17</sup> etc.; we began with the simplest.) The assumptions contained in these two equations are described in refs 13 and 18. The expression for the diffusion flux, for example, assumes that the particles take a random walk that is unaffected by other particles (dilute solution approximation), and it does not apply in systems in which the particles hop between a fixed number of sites.

Substituting the flux equations into eq 1 results in a PDE for the rate of change of the concentration of species  $i$  (the cations or the holes) at any location inside the polymer

$$\frac{\partial C_i}{\partial t} = -\nabla \cdot \vec{J}_i = -\nabla \cdot (-D_i \nabla C_i - z_i \mu_i C_i \nabla \phi) \quad (4)$$

In this framework,  $D_i$  and  $\mu_i$  are not constants but are functions of the oxidation level of the polymer. (It is possible that they are also functions of other variables, and part of the job of future modeling will be to determine the complete functional dependence of these coefficients.)

In systems at equilibrium with noninteracting particles that undergo random walks and that have a density given by the Boltzmann distribution,  $D_i$  and  $\mu_i$  are related through the Einstein relation:  $D_i/\mu_i = kT/q = RT/F$ .<sup>13,16,17</sup> In these systems, eq 4 is equivalent to the Nernst–Planck equation.<sup>11</sup> The advantage of the Einstein relation is that it reduces the number of independent coefficients that must be determined. Unfortunately, since diffusion during redox is not Fickian and since the density of the ions (or holes) is so high in the fully reduced (oxidized) states that they cannot realistically be considered to be noninteracting, this assumption cannot be made, and the model must examine the effect of a varying  $D/\mu$  (see section 4.3.2). For example, in systems with memory, in which the direction of a previous step affects the direction of the next step, the ratio  $D/\mu$  is concentration dependent.<sup>17</sup> A more general relationship is

$$\frac{D_i}{\mu_i} = \frac{C_i}{q \frac{\partial C_i}{\partial \eta}} \quad (5)$$

where  $\eta$  is the chemical potential. It has been shown that using this relationship with a Gaussian density of states accounts well for the increase in  $D/\mu$  with concentration seen in disordered organic semiconductors.<sup>19</sup>

Maxwell’s electrostatic equation (Poisson’s equation) is used to model the electric fields, giving the potential in terms of the net charge density  $Q$  ( $\text{C}/\text{cm}^3$ ).

$$\epsilon_0 \nabla \cdot (\epsilon \nabla \phi) = Q = \sum_{i=1}^n z_i C_i \quad (6)$$

Here  $\epsilon_0$  is the permittivity of a vacuum;  $\epsilon$  is the dielectric constant of the material; and  $z_i$  is the (positive or negative) charge of the ion or hole. In this paper, we used  $z_i = 1$  for both the holes and the ions and did not consider, e.g., divalent cations.

Equations 4 and 6 encompass the Nernst equation, which is derived by balancing the drift and diffusion terms at equilibrium. In fact, the formulation here is more general since the system is not at equilibrium during oxidation/reduction.

In this model, ion transport is not coupled to mechanical stress using a PDE (in the real system, ion ingress is responsible for volume change, and thus actuation stress in the polymer). Rather, this coupling is handled (section 5.1) artificially using an empirical form for the dependence of the diffusion coefficient on ion concentration, obtained in ref 4 (Figure 15). Coupling mechanical effects into the model, such as due to polymer stiffness, conformational changes, or actuation strain, should be the subject of future work.

**3.1.2.2. Boundary and Initial Conditions.** In the previous section, the treatment of the movement of charged species within the polymer was explained. To solve the PDEs of eqs 4 and 6, it is necessary to define boundary conditions (i.e., voltages, fluxes) and initial conditions. The boundary conditions (BCs) describe how the charges get in and out of the material, and they should correspond to the physical conditions imposed at the polymer/electrode and polymer/electrolyte interfaces. They

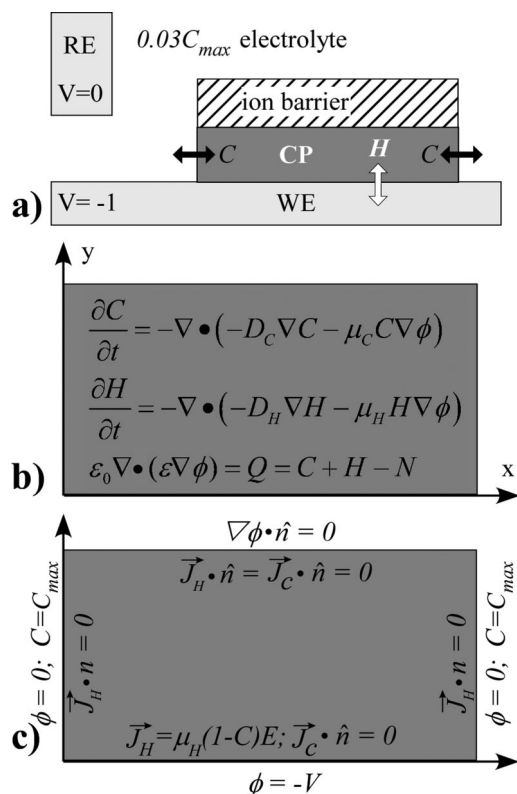


**Figure 1.** (a) Schematic of the physical system, showing the potentials on the working (WE) and reference/counter (RE) electrodes during electrochemical reduction of a cation-transporting polymer covered by an ion barrier, the bulk concentration of cations in the electrolyte ( $0.03C_{max}$ ), and the interfaces that ions ( $C$ ) and holes ( $H$ ) can cross. (b) The PDEs used in modeling this cation-transporting conjugated polymer. (c) The boundary conditions used at the polymer interfaces for a basic model that does not include ion transport in the electrolyte (the “base case” model of section 4).

must not only be chosen to make physical sense and lead to physically meaningful results but also they must allow the simulations to run.

At the polymer/electrode boundary, there is no ion flux across the interface, as shown in Figure 1 ( $\vec{J}_C \cdot \hat{n} = 0$ , where  $\hat{n}$  is a unit vector oriented perpendicular to the boundary). For the holes, a flux boundary condition was used at the electrode. During reduction, we set

$$\vec{J}_H = \mu_H H \vec{E} \quad (7)$$

With this expression, the higher the electric field  $\vec{E}$  and the higher the hole concentration  $H$  in the polymer, the higher the current density crossing from the polymer to the electrode. When the hole concentration falls to 0, current flow between the polymer and the electrode ceases. Since the simulation cannot solve for  $H$  if  $H$  is also used in the boundary condition, in the model this is actually phrased as  $\vec{J}_H = \mu_H(1 - C)\vec{E}$ , which is true almost everywhere by charge neutrality. This flux boundary condition was used in the 1D model. It could not, however, be used in the 2D simulations since it caused them to “crash”. Instead, the 2D model used a constant hole concentration  $C_0$  at the polymer/electrode boundary. To confirm that this gave the same results, the 1D model was run with the concentration BC and compared to the 1D model with the flux BC, and the results were the same. Furthermore, the results of the 1D and 2D simulations with  $C_0$  at the polymer/electrode interface were compared, and these results were also identical.

During oxidation, this boundary condition was changed to

$$\vec{J}_H = \mu_H C \vec{E} \quad (8)$$

because the current now depends on the number of available sites onto which a hole can potentially be placed, which is equal to the number of sites occupied by cations. The question arises as to whether to use the ion or hole mobility in these expressions since ion transport is the rate-limiting step. It turns out that using either  $\mu_H$  or  $\mu_C$  gives identical results.

The potential  $V$  at the electrode boundary in the model is, approximately, the applied *overpotential* in the experiments, i.e., the difference between the applied potential and the potential at which reduction (or oxidation) begins. This is distinct from the experimental applied potential (vs Ag/AgCl) because only fully oxidizing or reducing potentials can be applied in the model since the model does not yet take into account the energetics of charge transfer seen in the cyclic voltammogram. The electrode/polymer boundary condition used in the model is equivalent to stipulating that there is sufficient energy to allow the holes to cross the interface, in either direction, in response to the electric fields. Note also that in the model, setting  $\phi = -1$  V at the electrode and  $\phi = 0$  V at the electrolyte interface is equivalent to setting  $\phi = 0$  V at the electrode and  $\phi = +1$  V at the electrolyte, since only the potential *difference* is significant in the mathematics.

At the polymer/electrolyte boundaries, there is no hole flux ( $\vec{J}_H \cdot \hat{n} = 0$ ) since holes cannot enter the electrolyte. In the initial modeling cases (section 4), which do not include transport in the electrolyte, a constant ion concentration ( $C = C_{max}$ ) is imposed at the boundary during reduction, where  $C_{max}$  is the maximum concentration of ions in the polymer. (The effect of varying this boundary condition is shown in the Supporting Information, section 2.6.) Also in the initial cases, the potential at this interface is set to zero ( $\phi = 0$ ). This is not physically reasonable, since it ignores the resistive drop in the electrolyte, and thus causes the model to neglect the effects of changing

**TABLE 1: Nondimensional Units and Variables**

unitless variable	definition (from dimensional variables)	description	characteristic quantity used for normalization
$x, y, z$	$\mathbf{x}/L, \mathbf{y}/L, \mathbf{z}/L$	distance	$L$ = maximum ion path length
$\nabla$	$L\nabla$	gradient	
$\phi$	$\phi/V_0$	applied overvoltage on electrode	$V_0 = 1$ V
$C, H$	$C/H_{\max}, H/H_{\max}$	ion, hole concentrations in the polymer	$H_{\max}$ = maximum concentration in the polymer = number of immobile dopant anions
$t$	$t/[L^2/\mu_C V]$	time	$t_0 = L^2/\mu_C V$ = characteristic time = characteristic length /ion drift speed
$\partial/\partial t$	$[L^2/\mu_C V]\partial/\partial t$	time derivative	from definition of $t$ , by chain rule becomes unity through choice of $t_0$
$\mu_C$	1	cation mobility	$\mu_C$ = cation mobility
$\mu_H$	$\mu_H/\mu_C$	hole mobility	
$D_C$	$D_C/\mu_C V$	cation diffusivity	cation drift
$\epsilon$	$\epsilon V/L_0^2 H_{\max}$	dielectric constant	characteristic voltage gradient and charge concentration (using $z_i = 1$ )

electrical conductivity during redox. Therefore, in section 5.2 we expand the model to include the electrolyte.

The top polymer/insulator boundary has no ion or hole flux ( $\bar{J}_C \cdot \hat{n} = 0$  and  $\bar{J}_H \cdot \hat{n} = 0$ ), and it is electrically insulating ( $\nabla\phi \cdot \hat{n} = 0$ ). This boundary does not appear in the 1D simulations.

The initial conditions were an ion concentration of 0 and a hole concentration of  $H = H_{\max}$  everywhere, representing the fully oxidized state. The initial potential profile was found by solving the electrostatic PDE (eq 6) based on initial ion and hole concentrations.

**3.1.3. Reducing Model Complexity.** Two strategies were used to reduce the model complexity: (a) nondimensionalizing the model to reduce the number of free parameters and (b) reducing the number of spatial dimensions by exploiting symmetry or physics. Reducing complexity is important for running the models in a reasonable period of time, for reducing the number of independent parameters, and for running the models stably (i.e., without crashing). This leads to the introduction of the 1-D model that was used to generate most of the results in the paper and a description of how this relates to the physical system. Finally, we describe the transformation of the numerical values of the physical system described in ref 4 to the nondimensional values used throughout the simulations.

**3.1.3.1. Nondimensionalization.** Nondimensionalizing (i.e., normalizing) the model reduces the number of parameters to those that are actually independent. The nondimensional parameters better illustrate the balance between competing physical effects since each nondimensional parameter represents a ratio of dimensional parameters, and they allow a single modeling run to predict the behavior of a whole range of dimensional parameters. An excellent discussion of the benefits of nondimensionalization is provided in ref 20.

Essentially, each dimensional variable is normalized by a characteristic scale of the system (see Table 1). For example,

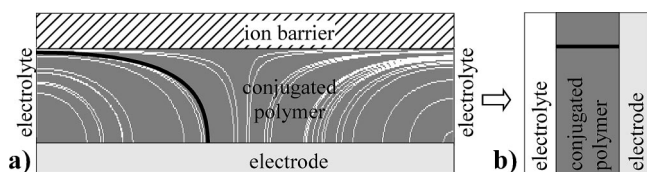


**Figure 2.** (a) A schematic 2-D slice across an ion-barrier-covered, oxidized PPy(DBS) strip at  $t = 0$ , showing calculated electric field lines (white) going from the electrode to the electrolyte prior to any ion ingress. The 1-D model can be considered to represent ions and holes traveling along one of these field lines (such as indicated by the black line). For clarity, the vertical axis is much exaggerated in comparison with the experimental geometry. (b) The geometry studied in the 1-D models is equivalent to a line between the electrolyte and the electrode.

the nondimensional length  $x$  was obtained by taking the dimensional length  $\mathbf{x}$  ( $\mu\text{m}$ ) and dividing it by the maximum ion path length  $L = 150 \mu\text{m}$ , a length that characterizes the size of the experimental system, so  $x = \mathbf{x}/L$ . The boldface variables denote dimensional quantities, and the plain text variables denote nondimensional variables. Ion and hole concentrations were nondimensionalized by  $C_{\max} = H_{\max} = 3$  M, the estimated maximum concentration of ions/holes in the polymer. All nondimensional variables are unitless. The nondimensionalization of the remaining variable and the resulting PDEs are derived in the Supporting Information (SI section 1.1).

The nondimensional governing equations for cation and hole transport are

$$\begin{aligned}
 \text{(a)} \quad \frac{\partial C}{\partial t} &= -\nabla \cdot (-D_C \nabla C - C \nabla \phi) \\
 \text{(b)} \quad \frac{\partial H}{\partial t} &= -\nabla \cdot (-D_H \nabla H - \mu_H H \nabla \phi) \\
 \text{(c)} \quad \nabla (\epsilon \nabla \phi) &= Q = C + H - 1
 \end{aligned} \tag{9}$$

where  $\mu_C$  is not shown in the first equation because it is equal to 1. The dimensional model, eqs 4 and 6, has eight free parameters:  $D_C$ ,  $\mu_C$ ,  $D_H$ ,  $\mu_H$ ,  $\epsilon$ ,  $V$ ,  $L$ , and  $H_0$ . The nondimensional model, eq 9, has four:  $D_C$ ,  $D_H$ ,  $\mu_H$ , and  $\epsilon$ .

**3.1.3.2. Reduced Spatial Dimensions.** PDEs are solved in finite element models by meshing the computational region in space into cells (nodes) and then iterating all the variables (ion and hole concentrations and electric potential) in time across all the spatial nodes. Increasing the number of spatial dimensions increases the computational cost, by the square in going from 1-D to 2-D and by the cube in going to 3-D. Therefore, we started with fast-running 1-D models for initial model development (less than 1 min of run time) and proceeded to 2-D models (20 to 30 min of run time) once we were satisfied with the qualitative predictions. By the symmetry of the experimental geometry, which had no variation along the long axis of the polymer stripe, 3-D models were not required.

The 1-D models were numerically more robust than the 2-D models because they had fewer nodes and required less computer memory. The 2-D models, operating near the limit of computer memory and speed, were more fragile, “crashing” in several cases, such as when large gradients were created that were not well resolved by the mesh. In addition, when numerical issues arose, such as resolving steep gradients, including sharp cutoff functions to prevent the charge from going above  $C_{\max}$  or  $H_{\max}$  (charge capping), or capturing small dielectric coefficients, the 1-D models could be solved by increasing the mesh resolution.

At  $t = 0$ , the electric field lines form arcs through the polymer between the electrode and the electrolyte. Conceptually, the 1-D

simulation can be considered to be along one of these lines, as shown in Figure 2. Note that this is the case because no nucleation occurs in PPy(DBS). To simulate nucleation in polymers such as PPy(CIO<sub>4</sub>), in which ion ingress begins along vertical lines,<sup>21</sup> a 2-D or 3-D model would be needed.

Figure 2b is the same geometry as for a layer of conjugated polymer on an electrode uncovered by an ion barrier, so the model should correctly predict the behavior for this case as well. The question arises, how much does the transport differ in the ion-barrier covered case, due to the distortion of the field lines, from the thin film case? This question is taken up in section 4.2, in which the 1-D simulation is compared to a 2-D simulation.

**3.1.3.3. Parameters.** Of the eight dimensional model parameters ( $D_C$ ,  $\mu_C$ ,  $D_H$ ,  $\mu_H$ ,  $\epsilon$ ,  $V$ ,  $L$ , and  $H_0$ ), three are known:  $V$  is 1 V,  $L$  is 150  $\mu\text{m}$ , and  $H_0$  is 3 M. The static dielectric constant  $\epsilon$  depends on the doping level, varying between 4 in the undoped state (close to typical values for polymers) to 1000 in the fully doped state for polyaniline;<sup>23</sup> values are similar for doped PPy.<sup>22</sup> (The dielectric constant also depends strongly on temperature and frequency.<sup>22</sup>)  $D_C$  and  $\mu_C$  only come into the model as a ratio, and initially a ratio of 0.026 was used, taken from the Einstein relation  $D/\mu = kT/q = 0.026 \text{ V}$ .<sup>13</sup> The coefficients for the holes were defined relative to those for the ions, and in the baseline model case (section 4.1), they were taken to be 1000 times larger, so  $D_H = 26$  and  $\mu_H = 1000$ . The choice of the factor of 1000 was somewhat arbitrary: it is known that hole transport is much faster than ion transport but not by how much. The choice of 1000 was enough to make hole transport virtually infinitely fast relative to ion transport for the configuration used in ref 4.

**3.2. Numerical Methods.** This section discusses the methods used to solve the equations, as well as the computational issues that were encountered (meshing, stability) and how they were overcome. For example, the ways we handled the inability to use a physically reasonable value for the dielectric constant is described.

**3.2.1. General.** The nondimensional PDEs were solved using the PDE modeling software FEMLAB (COMSOL), version 3.2. Of the three PDEs in eq 9, the first two are dynamic (they contain time derivatives  $d/dt$ ), and the last one is static. We proceeded by choosing initial conditions for  $C$  and  $H$  at  $t = 0$  and solving the electrostatic PDE for the potential  $\phi$  that satisfied the boundary conditions. Using starting variables  $C(x,y,t = 0)$ ,  $H(x,y,t = 0)$ , and  $\phi(x,y,t = 0)$ , FEMLAB then solved the PDEs at each time step and updated the variable values to find  $C$ ,  $H$ , and  $\phi$  at  $t = \Delta t, 2\Delta t, 3\Delta t, \dots, T$ , where  $T$  is the simulation end time.

We used a number of techniques to enable and improve the numerical simulations since numerical solution schemes for drift/diffusion PDEs can suffer from numerical instability and spurious oscillations, particularly in simulations with sharp propagating fronts. As is standard in numerical methods, a small amount of artificial diffusion was added to stabilize the simulations (this does not change the character of the solutions). Specifically, we added the Petrov–Galerkin compensated artificial diffusion available within FEMLAB<sup>24</sup> to both hole and ion transport (using a tuning parameter of 0.25). For consistency, we used this in all the simulations, even in cases that already had a significant amount of diffusion.

The smaller the dielectric constant  $\epsilon$ , the smaller the regions in which charge neutrality is violated. For the experimentally reasonable values of  $\epsilon$  given above, the nondimensional dielectric constant  $\epsilon$  is on the order of  $10^{-11}$ , yielding regions

that are so thin that the mesh density required to resolve them was beyond our computing capabilities, even for the 1-D model. Therefore, the models were run with the smallest dielectric constant that could be resolved,  $\epsilon = 10^{-3}$ . We then verified that as  $\epsilon$  decreased the behavior of the model converged (Supporting Information section 2.1, or SI 2.1). We also ran cases with charge neutrality strictly enforced ( $\epsilon = 0$ ). (In the Supporting Information, we show how the charge-neutral equations can be derived from the governing equations 9a–c, and we show that the charge-neutral behavior is exactly the limit of the small- $\epsilon$  behavior as  $\epsilon \rightarrow 0$ .)

**3.2.2. 2-D Simulations.** For the 2-D simulations, there were additional computational issues. First, finer meshing was needed in regions where the electric field changed rapidly. This was done, after solving for the initial potential, by allowing FEMLAB to adapt the mesh spacing given that potential profile and using the same mesh in all subsequent simulation steps. (This mesh is thus optimized for the potential profile at  $t = 0$  and not for later times. This means that the mesh will not be optimized during the entire simulation since FEMLAB cannot perform real-time adaptive meshing.)

Second, the 2-D the geometry posed some additional challenges. In the experiments, the thickness of the polymer (300 nm) was small compared to its half-width (150  $\mu\text{m}$ ), giving an aspect ratio (height:width) of 1:500. This configuration could not be used directly because it was numerically unstable: if the thickness ( $z$ -direction) was discretized into 10 nodes and the width ( $y$ -direction) into 100 nodes, then each grid element had an aspect ratio of 1:50 (= 0.03/1.5). However, numerical errors increase as mesh elements deviate away from an aspect ratio of 1. To address this problem, the simulated film thickness was instead set to be 100 times thicker than the actual film thickness and both directions discretized into 100 nodes, so that the grid elements had an aspect ratio of 1:5. To correct for the increased thickness,  $D$ ,  $\mu$ , and  $\epsilon$  in the  $y$ -direction (thickness direction) were increased, creating anisotropic diffusion, migration, and dielectric coefficients and making the film act as if it were thinner. To compensate for the 100-fold increase in thickness, these parameters should have been increased by a factor of 100<sup>2</sup>, with the square arising from the spatial second derivatives in eq 9. However, the largest anisotropy for  $D$  and  $\mu$  that was stable in the simulations was 1000. Thus, the simulation geometry was equivalent to a film with an aspect ratio of 1:158. The dielectric constant was only increased by a factor of 10 (giving at least some degree of anisotropy) since it was already too large, and increasing by 10 000, it would have moved  $\epsilon$  even further away from realistic values.

With boundary conditions as shown in Figure 1c, the sharp square corners, where the electric fields become highly concentrated, led to numerical instabilities. The electrode/electrolyte and ion-barrier/electrolyte corners were therefore beveled to a 45° angle. Also, with two different potentials applied at the polymer/electrode and polymer/electrolyte interfaces, there was a voltage step at the vertices (see Figure 1c). Experimentally, this does not arise because the electrolyte is not a perfect conductor, and the voltage at the corners will blend smoothly from  $\phi = -V$  (polymer/electrode) to  $\phi = 0$  (polymer/electrolyte). An exponential decay was used in the simulations to smoothly change the voltage from the electrode/electrolyte corner to the electrode edge.

## 4. Results 1: Base Case Model and Variations

In this section, we present the results of running a simplest case model so that its basic behavior can be understood, i.e.,

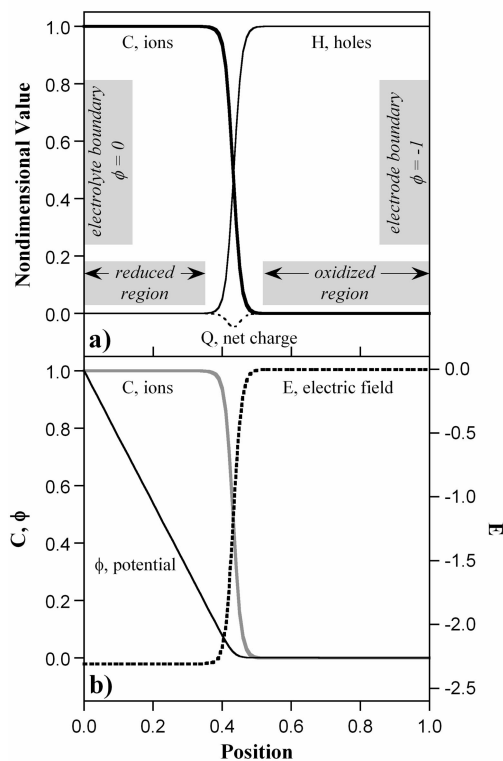


**Figure 3.** Snapshot during the reduction process in the base case model. (a) Ion, hole, and net charge concentrations as a function of position. (b) The corresponding potential and electric field, with the ion concentration shown in gray for comparison. Note that the electric field has a different scale.

not only what the model predicts but also why, before complexities like an electrolyte layer are added. As we show below, this model is sufficient to describe most of the results seen experimentally during the reduction of a PPy(DBS) stripe covered with an ion barrier. The benefits of running simple models include transparency in understanding the outcomes as well as faster and more robust simulations. However, as we shall show in later papers, other experimental geometries require more sophisticated models.

As discussed above, the model was built based on electrochemical reduction of a cation-transporting material. To begin the modeling effort, we started with a base case, which was the simplest case, and then increased the model complexity step by step, proceeding to the more difficult, and realistic, cases. This section is thus presented as a theme (the base case) with variations, the latter being used both to confirm that the model was behaving reasonably, i.e., predicting behavior that was qualitatively consistent with the experiments, and to give a firm understanding of how the model behaved and why. Results are primarily from the 1-D model, with 2-D simulations run when necessary for confirmation. After this, the model complexity was increased by adding nonconstant coefficients as well as transport in the electrolyte.

Since the base case is the simplest, it only includes transport in the polymer (not in the electrolyte yet). As mentioned above, the material coefficients  $D_C$ ,  $D_H$ ,  $\mu_C$ ,  $\mu_H$ , and  $\epsilon$  depend on the state of the polymer; they can be functions of ion concentration  $C$ , hole concentration  $H$ , and the electric potential  $\phi$ . However, in the base case, these coefficients were all treated as constant.

**4.1. Base Case Simulation Results.** Figure 3a shows the ion and hole concentrations and the net charge as a function of position along the line in Figure 2b partway through the

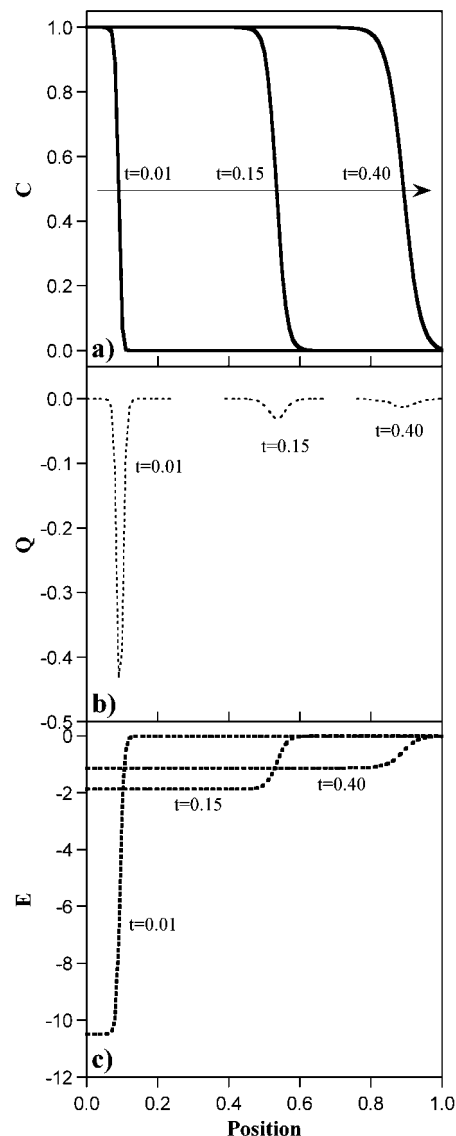


**Figure 4.** At three times during reduction in the base case, the (a) cation concentration, (b) net charge, and (c) electric field.

reduction process with an electrode potential  $\phi = -1$ . As in that figure, the electrolyte is on the left and the electrode on the right; this will be the case in all the figures in this paper.

There are several things to note in Figure 3. The reduced material is on the left, since the cations enter from that side, the oxidized material is on the right, and there is a front between them. The nondimensional ion concentration  $C$  on the left is 1, which means that the material is completely reduced, and it transitions to zero at the front. The hole concentration  $H$  goes the opposite way, from zero on the left to 1 on the right, corresponding to fully oxidized material. The ion and hole concentrations mirror each other because they are tied together through eq 9c. (For this reason, in a simulation in which holes were not permitted into the polymer from the electrode side, the material did not reduce: nothing further happened after a small initial build-up of holes at that interface.) Note, however, that there is a small net charge at the front. It is negative, showing that in this region the retreating holes have not been completely replaced by cations. The holes cannot leave the material any faster than the ions can arrive (or the net charge and electric fields would grow without limit), and as will be shown below, the velocity of the front is thereby limited by the ion speed. Another thing to observe is that with the parameter

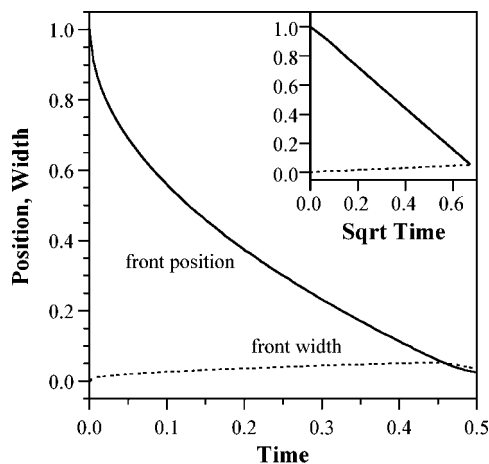


**Figure 5.** Front position and broadening vs time during reduction in the base case. Both go as the square root of time (see inset). The front broadening curve was obtained by averaging three simulations with different meshes to reduce numerical noise.

settings of the base case the migration component of the flux makes a substantial contribution to the transport, as evidenced by the existence of a front. (Since we are using constant coefficients with a Fickian diffusion equation, the front cannot arise from the diffusion component.)

To relate these curves to the experimental work, the ion concentration should be compared with Figures 5 and 7 in ref 4 (see also ref 9). The ion concentration in Figure 3a, when mirrored around the  $y$ -axis, corresponds to intensity in the experimental profiles. There is good qualitative agreement.

Figure 3b shows the electric field and the potential at the same instant of time. There is almost no potential drop across the oxidized region of the film; instead, the voltage is dropped across the reduced region. This is the result one would expect from a consideration of nondimensional material conductivity, given by

$$\sigma(x) = C(x)\mu_C + H(x)\mu_H \sim H(x)\mu_H \quad (10)$$

since  $\mu_H/\mu_C = 1000$ . In the model, this outcome arises automatically from the transport equations. The cation and hole fluxes due to migration are expressed as  $J_C^{\text{drift}} = z_C\mu_C C_c E = \sigma_C E$  and  $J_H^{\text{drift}} = z_H\mu_H C_H E = \sigma_H E$  (where  $z_C = z_H = 1$ ). Therefore, the migration current density is

$$J^{\text{drift}} = (\sigma_C + \sigma_H)E \quad (11)$$

which is immediately recognizable as a variant of Ohm's law. Thus, in Figure 3b the voltage drop is linear with position in the fully reduced region since this area behaves essentially as a resistor.

The results obtained from using eq 9b with  $\mu_H/\mu_C = 1000$  are virtually the same as were obtained from using an analytical equation for the holes, published in ref 10. The two sets of curves are plotted together in the Supporting Information, SI 2.2.

Figure 3 showed a single snapshot in time, but how do these curves evolve, and how fast does the front travel? Figure 4a shows the ion concentration profile at three times. Initially, the front, at which the ion concentration drops from 1 to 0, is narrow, with the curve nearly vertical. As the front travels into the film, it broadens, and the "foot" at the base goes from an abrupt, nearly 90° turn to a concave curve.

The net charge  $Q$  at these times is shown in Figure 4b, and the electric fields in Figure 4c. The net charge does not remain

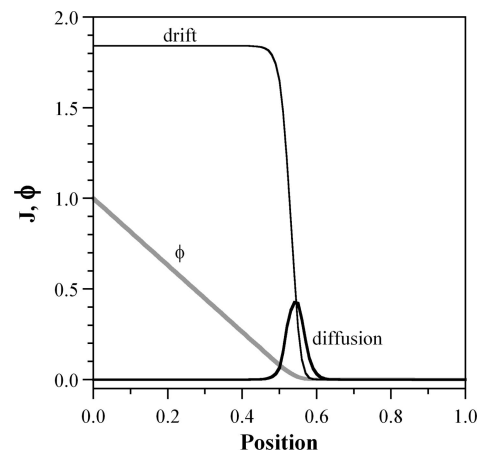


**Figure 6.** Diffusive and drift components of the ion flux at  $t = 0.15$  during reduction in the base case model, with the potential indicated in gray for reference.

constant as the front propagates, but diminishes. Its magnitude is determined by  $\hat{\epsilon}$ , which is constant, and by the gradient of electrical field across the front, which decreases over time due to broadening.

By analogy with the Haynes–Shockley experiment,<sup>13</sup> one could attribute front movement to drift and front broadening to diffusion. In silicon, the front velocity is constant, and the front broadens with the square root of time. It is clear from the time labels in Figure 4a, however, that the front in the conjugated polymer does not move linearly with time. This is because the doping in inorganic semiconductors is constant, whereas the doping level in conjugated polymer changes, so the electric field is not constant.

The front position and width are shown as a function of time in Figure 5. The front position  $x$  was defined as the position at which the ion concentration is 0.5, and the front width was the distance between the positions at which the ion concentrations are 0.25 and 0.75. Both the front position and broadening have a  $\sqrt{t}$  dependence. The total number of ions, obtained by integrating the ion concentration profile, corresponds to the experimental average intensity; this also increases with  $\sqrt{t}$ , matching the experimental result (Figure 19 in ref 4). The current is obtained from the time derivative of the total number of ions in the film and therefore goes as  $1/\sqrt{t}$ . (It should be noted that the simulation current does not, of course, include capacitive or parasitic currents.)

The reason for the square root of time dependence of the front position is that the voltage is dropped primarily across the insulating region, which grows wider as the reduction front propagates; thus, the electric field in the insulating region,  $E = dV/dx$ , drops. To explain the  $\sqrt{t}$  dependence, we reason thusly. The velocity of ions  $v_C$  under migration is given by  $v_C = \mu_C E$  everywhere in the film. The velocity of the front is essentially the velocity of the ions  $d\bar{x}/dt \approx v_C$ , where  $\bar{x}(t)$  denotes the front location versus time. Since the potential drops linearly with position in the reduced region,  $E = V/\bar{x}$ . Substituting,  $d\bar{x}/dt \approx v_C = \mu_C V/\bar{x}$ . In the base case,  $\mu_C$  is constant, and since  $V$ , the applied potential, does not change during the reduction process, it is also constant. The solution is therefore  $\bar{x} = \sqrt{2\mu_C V} \sqrt{t}$ . *The square root dependence arises entirely from migration and has nothing to do with diffusion; it is due to the way the front advances and takes the film from conducting to insulating.* This must be kept in mind when interpreting experimental results.

It is instructive to separate the ion flux into diffusive and drift components, as shown in Figure 6. In the reduced region,

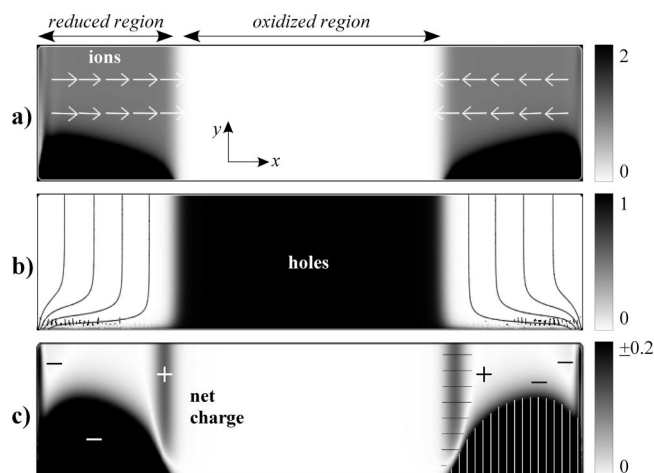


**Figure 7.** Concentration profiles resulting from running the base case in a 2-D simulation with  $V = -1$ . (a) Ion concentration, indicated by gray scale intensity; the gray in the reduced area corresponds to  $C = 1$ . The arrows show the electric field direction and strength. (b) Hole concentration  $H$ , with the lines showing contour plots of constant potential. (c) Net charge ( $C + H - 1$ ), shown with a magnified gray scale for clarity. Positive and negative net charge are both indicated by dark shading. On the right, positive net charge is indicated by horizontal hatching and negative net charge by vertical white hatching.

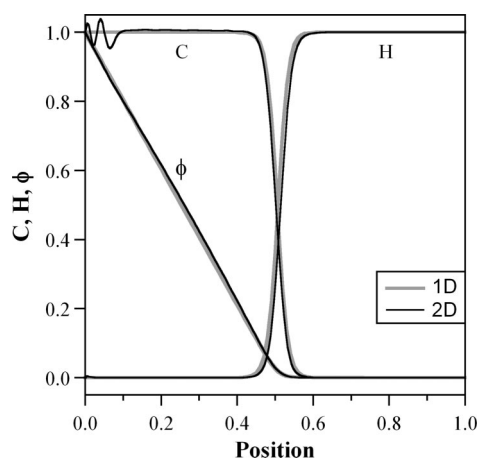


**Figure 8.** Comparison of ion, hole, and potential profiles from the 1-D and 2-D simulations at the same electrochemical reduction level. (The wiggles in the 2-D ion profile on the upper left are from numerical noise.)

the cations move solely by drift: there is no concentration gradient, so the diffusion term is zero. Only at the front, where the concentration gradient is located, do they diffuse. This result, together with the others for the base case, shows that the model is functioning properly and behaving reasonably and that our hypothesis that front movement is by drift and front broadening by diffusion is correct.

**4.2. 2-D Confirmation of 1-D Results.** Before varying the base case parameters, it was important to check that the 1-D simulations had given essentially the same results as a full 2-D simulation (as claimed in Figure 2a). Therefore, the base case was run in 2-D. Figure 7 shows snapshots of the ion, hole, and net charge concentrations halfway through the reduction process. As in the 1-D case, the ions entered the film as a front, with a net negative charge between them and the holes.

One important thing to note in Figure 7a is the electric field direction. After time  $t = 0$  (shown in Figure 2a), the field lines become parallel with the bottom electrode, leading the ions inward in a straight line. The field magnitude is constant in the

reduced area and drops to almost zero in the oxidized area. Correspondingly, the lines of constant potential Figure 7b are uniformly spaced in the reduced region, showing that the potential drops linearly along  $x$ , and the lines are vertical, showing that along the film thickness the potentials are essentially constant. As a consequence, the 1-D and 2-D simulation results are virtually identical, as shown in Figure 8. The Supporting Information (section 2.4) shows that the front velocity in the two models is almost the same. (Note that a scaling factor for time was needed when comparing the 1-D and 2-D results. The Supporting Information contains a mathematical derivation of this factor.)

It should be noted that the fields are distorted at the bottom electrode, as seen in both the ion concentrations and the potential contours. The reasons for this are 2-fold. One is the too-large dielectric constant that had to be used in this simulation, which allowed the net positive charge to grow to high values (up to 2 at the bottom edge). (By eq 9c, the larger the value of  $\epsilon$ , the larger the allowed charge imbalance.) The second was the high field concentrations at the corners, caused by the jump in the  $\phi$  boundary conditions shown in Figure 1c. Only the upper portion of the simulated film was therefore used to derive Figure 8.

Physically, the ion and hole concentrations in the polymer do not exceed  $C_{\max}$  or  $H_{\max}$  because the maximum number of polarons is approximately 1 per every 3–4 monomer units in PPy; removing additional electrons requires much higher voltages and results in reactive cation radicals that lead to polymer degradation. Our model does not yet, however, include either the chemistry or energetics that could enforce this limit. Therefore, to limit the concentrations of ions and holes, the results in Figure 7 were obtained by “capping” the ion and hole concentrations by setting the migration term to zero when either concentration went above 1. In effect, this turns off the electric field in regions of too-high charge concentration, removing the forces that pull the charges there and allowing them to diffuse away rapidly, down the large concentration gradients. This was implemented by multiplying the migration term with a step function. (Recall that the number of holes reversibly removed from the polymer during reduction is equal to the number added during oxidation. The number of cations in the reduced polymer cannot exceed the number of holes that were removed without violating charge neutrality, so  $H_{\max} = C_{\max}$ . (Locally, there may be small amounts of net charge, violating charge neutrality. However, even a small net charge creates large electric fields. Small amounts of net charge are neglected in this argument, which concerns large charge imbalances.) Thus, when the polymer is fully oxidized,  $H = H_{\max}$  and  $C = 0$ , and when it is fully reduced,  $H = 0$  and  $C = C_{\max}$ . In the physical system, removing more than  $H_{\max}$  electrons results in irreversible chemical reactions rather than more holes. The model, however, does not include such considerations, and thus, without capping,  $H$  and  $C$  reached unrealistically high values in 2-D simulations. This method of enforcing physically reasonable concentrations in the polymer is itself unphysical, in that it does not correspond to a physical process for regulating the charge. However, since this model included neither the energetics of charge injection nor a sufficiently small dielectric constant, it was necessary to resort to this stratagem.)

**4.3. Parameter Variation.** In this section, the outcomes from varying the base case parameters are presented so that their roles in the basic model can be fully understood. Only one parameter is varied at a time, with the others kept the same as in the base case. Once the effect of these variations is clear and the reasonableness of these results is confirmed, then the model

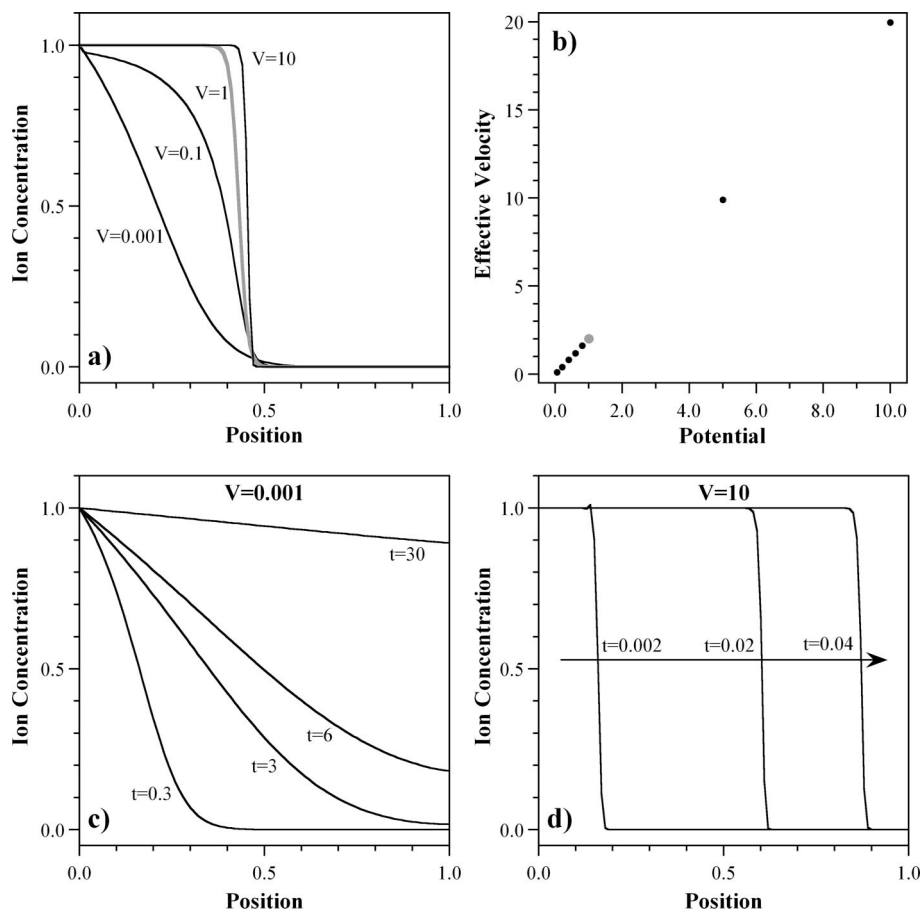


**Figure 9.** (a) Ion concentration profiles for a range of reducing voltages applied at the polymer/electrode boundary in the base case model. The profile with the standard base case parameters is indicated by the gray line. (b) Front velocity as a function of voltage. (c) Ion profiles at different times for  $V = 0.001$ . These ion concentration profiles are similar to those obtained when the ions move under diffusion only (compare to Figure 15). (d) Ion profiles at different times for  $V = 10$ , which is essentially a migration-only case.

complexity can be increased to represent the experimental configuration more realistically.

**4.3.1. Voltage.** Changing the voltage at the polymer/electrode boundary corresponds to changing the applied overpotential in the experiments. Experimentally, changing the applied potential dramatically changed the behavior: at low voltages, there was no ion front, but a front emerged as the voltage was increased. Furthermore, experimentally the front velocity was linearly dependent on the applied voltage. The first real test of the model is thus its ability to correctly reproduce these results. The model was run with potentials at the boundary varying between 0.001 and 10.

Figure 9a shows that lower-voltage profiles are broader, and the ions move more slowly. In fact, when the voltage is close to zero, at  $V = 0.001$ , the ion concentration profile has no front. This happens because the diffusion and drift terms add linearly in the transport PDEs. The drift term increases linearly with the field, and thus at each point in the material it increases linearly as the voltage is raised. Changing the voltage therefore dials the size of the drift term relative to the diffusion term. The net charge at the front also decreases when the reduction potential is lowered, as shown in SI 2.3, because lowering the potential lowers the gradient of the electric field, to which  $Q$  is proportional by eq 7c.

To qualitatively compare the experimental data with the simulation results, see Figure 7 in ref 4. The agreement is striking.

In Figure 9b, the front velocity is plotted as a function of the voltage. Since the velocity decreases with time, an *effective*

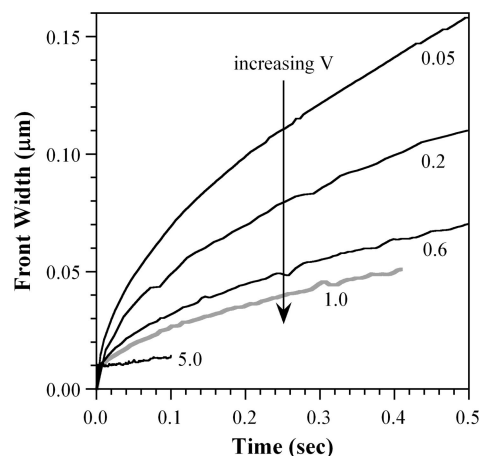


**Figure 10.** Front width versus time at different applied potentials (indicated) during reduction obtained using the base case model.

*velocity* had to be plotted. This was taken as the distance traveled by the front divided by the time it took to get there, where the distance that was used was from the electrolyte to the electrode (1 in normalized distance), and the front position was, as above, the point at which the ion concentration was 0.5. The effective front velocity was linear with voltage, as occurred in the experiments (Figures 10 and 11, ref 4).

One limiting case arises when the voltage is turned off completely, giving a profile for diffusion only, and another arises when the voltage is very high, giving a profile for drift only.

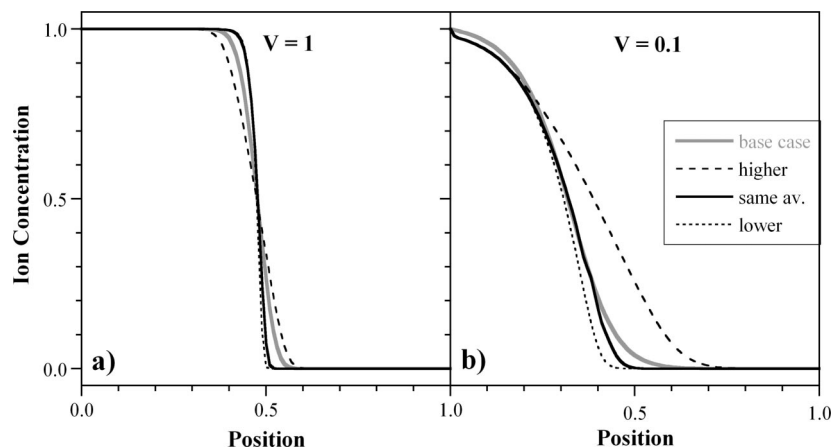


**Figure 11.** Ion concentration profiles in the base case model during reduction when  $D_C/\mu_C$  is not constant (base case, gray line) but proportional to  $C$  (other lines). (a)  $V = 1$ ,  $t = 0.12$ . (b)  $V = 0.1$ ,  $t = 0.52$ .

(The potential cannot be set identically to zero in the model, so a very small value of  $V$  was used instead,  $V = 0.001$ .) Under diffusion only, ions initially enter the polymer rapidly (see  $t = 0.3$ , Figure 9c), forming something like a front (i.e., the part of the film on the left is reduced and the part on the right is oxidized). A short time later, however, the polymer is partially reduced everywhere. The ion concentration at  $x = 0$  stays fixed at 1 by the boundary condition, and the level throughout the rest of the polymer gradually rises. The polymer requires a long time ( $t > 30$ ) to become fully reduced. In the limiting case of migration only ( $V = 10$ , Figure 9d), there is a definite front, on one side of which  $C = 1$  and on the other side of which  $C = 0$ , that moves into the film. This front broadens very little over time.

If the front broadening was due only to Fickian diffusion, then it would not depend on the potential. The front width as a function of potential is shown in Figure 10, and there is a strong voltage dependence. (The front broadening decreases approximately as  $1/\sqrt{V}$ , as shown in SI Figure SM5). This finding is in contradiction to the experimental data (Figure 13 in ref 4), indicating that this base case model does not handle the front broadening properly.

The front broadening in the model is under the influence of both diffusion and migration. Diffusion tries to increase the front width to lower the concentration gradient, while migration decreases the front width to lower the net charge. The migration term increases with the overpotential  $V$ , and the front broadening is thus found to be slower, as expected.

**4.3.2. Relationship between  $D$  and  $\mu$ .** Another, essentially equivalent, way to vary the relative contribution of the diffusion and migration terms in the base case model, in which the diffusivity and mobility are constant, is through their ratio. This was set to  $D/\mu = 0.026$  for both ions and holes in the base case, where that value arose from assuming that the Einstein relation was valid. Increasing the ratio has the same effect as lowering the reduction potential (as shown in SI section 2.9). Also, as pointed out previously, since the density of ions (or holes) is so high in the fully reduced (oxidized) state that the charges cannot realistically be considered to be noninteracting, the assumption that the Einstein relation is valid cannot be made blindly, and the model must examine the effect of a varying  $D/\mu$ .

We therefore examined how varying the  $D/\mu$  ratio based on the more general relationship between diffusivity and mobility given in eq 5 changed the concentration profiles. Specifically, Figure 11 shows the effect on the ion profile if  $D_C/\mu_C$  is

proportional to  $C$ . Since it is not clear how to choose the magnitude of this function to best compare with the base case, three relationships were used: (1)  $D_C = 0.026(1 + 5C)$ , (2)  $D_C = 0.026(1 + 5C)/3.5$ , and (3)  $D_C = 0.026(1 + 5C)/6$  ( $\mu_C = 1$  for all cases). The first gives the same minimum  $D/\mu$  but an averaged (over concentration)  $D/\mu$  that is 6 times higher than the 0.026 of the base case; the second gives the same average  $D/\mu$ ; and the third gives  $\sim 2$  times lower average  $D/\mu$  but the same maximum  $D/\mu$ , thereby bracketing the base case. In Figure 11, these three relationships are noted as higher, same, and lower, respectively.

For  $\phi = -1$ , the speed of the front is not significantly changed by the alteration in  $D_C/\mu_C$  because front propagation speed is dominated by migration, so a variation in the diffusivity has a negligible effect. The front width is affected, however. For the relationship labeled “same av.,” the front is narrower than the base case, particularly at the foot where  $C$  is small. The difference between “same” and “lower” is also seen at the foot, becoming even sharper for the latter. For “higher,” the front is broader everywhere. The same basic behavior was seen for  $\phi = 0.1$ . Thus, using a more general relationship between  $D_C$  and  $\mu_C$  only has a minor effect on the simulation predictions, and one that would be difficult to observe experimentally.

**4.3.3. Finite Hole Mobility.** Whether the electron movement or the hole movement is rate-limiting depends on their relative mobility. Experimental studies have suggested that hole transport is orders of magnitude faster.<sup>25–27</sup> Even so, hole transport may be the rate-limiting step in some experiments.<sup>28–31</sup> The value of adding eq 9b to the model, over our prior work in which an analytical equation was used, is that it allows us to examine such cases.

The ion concentration profile resulting from setting the hole mobility equal to the ion mobility is shown in Figure 12a in comparison with the base case, in which hole mobility was 1000 times higher. (Additional ion concentration profiles can be found in SI section 2.5.) The corresponding potentials as a function of position are shown in Figure 12b.

The voltage profile changes significantly, now dropping linearly between 0 and 1. This can, of course, be seen by examining eq 10: since the conductivity and charge density of the oxidized and reduced regions are now identical, Ohm’s law dictates a constant potential drop over the whole film. The resulting smaller potential drop over the reduced region compared to the base case lowers the front velocity. The front is also wider than in the base case since the electric field is

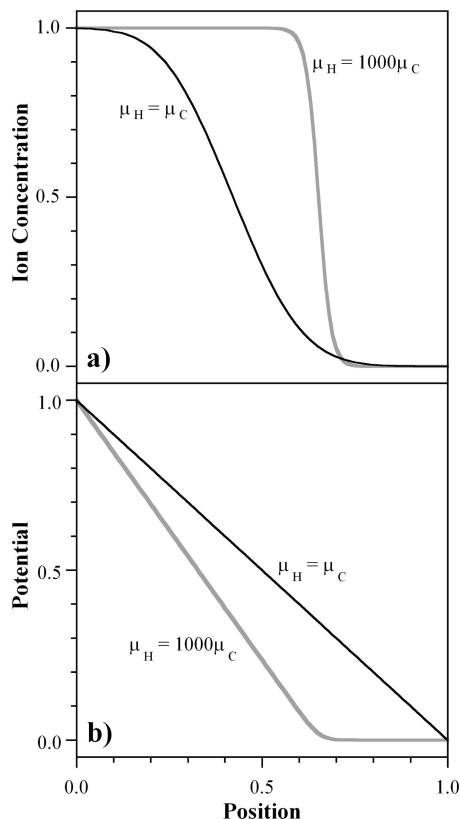


**Figure 12.** (a) Ion concentration profiles when the hole mobility is set equal to the ion mobility during reduction. The gray line shows the base case with the usual 1000:1 ratio of hole mobility to ion mobility at the same time ( $t = 0.22$ ). (b) The corresponding potential profiles.

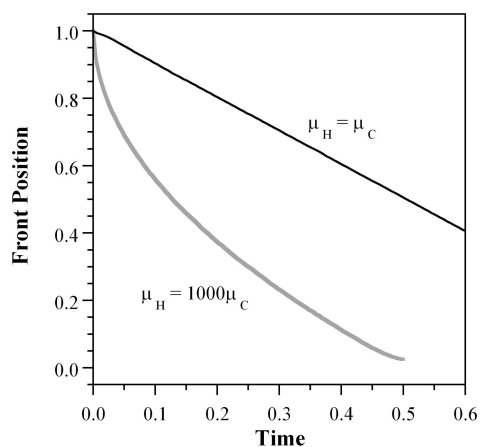


**Figure 13.** Position of the front vs time when the hole mobility is set equal to the ion mobility during reduction. The gray line shows the usual base case result.

smaller, which allows diffusion to broaden the fronts more quickly (see Figure 10).

As a general rule to understanding the simulation results, the key is the potential profile that develops in the polymer under different conditions. Lowering the hole mobility, changing the boundary conditions, or introducing concentration-dependent coefficients changes the potential profile and thus the charge transport.

The front position is shown as a function of time in Figure 13. As noted above, the front moves more slowly when the mobilities are equal, but more importantly the velocity is *constant*, a direct result of the unvarying potential across the

film. In PPy(DBS), there is 4 orders of magnitude difference between the conductivities in the oxidized and reduced states,<sup>32</sup> so this probably does not explain the experimental results in ref 4 Figures 8 and 9. However, this case might be observed in other systems having poor hole mobility arising from defects or other energy barriers. A change from  $\sqrt{t}$  to  $t$  might also occur upon polymer degradation, which would have the effect of lowering the conductivity of the oxidized state.

**4.3.4. Charge Neutrality Strictly Enforced.** The argument can be made that charge neutrality cannot be violated during redox in a conjugated polymer because the high hole mobility will produce near-perfect charge shielding. Equation 9c was therefore modified as follows to explore the effect of enforcing zero net charge:

$$\nabla \cdot (\mu_C C \nabla \phi + \mu_H H \nabla \phi) = 0 \quad (12)$$

This formulation is found by setting  $\varepsilon = 0$  in eq 9c and dropping the now unnecessary hole transport eq 9b (in the charge neutral case, holes track ions, so it is not necessary to have an equation for them). Manipulating eqs 9a and b, using the charge neutral constraint of  $\varepsilon = 0$  in 9c, leads to eq 12, which together with 9a is the charge neutral model (see SI section 1.2). (To get eq 12, add the hole and ion transport equations, giving  $\partial[C + H]/\partial t = -\nabla \cdot [(-D_C \nabla C - \mu_C C \nabla \phi) + (-D_H \nabla H - \mu_H H \nabla \phi)]$ . By charge neutrality, we have  $H + C = 1$ . Substituting,  $-\nabla \cdot [(-D_C \nabla C - \mu_C C \nabla \phi) + (-D_H \nabla H - \mu_H H \nabla \phi)] = 0$ . Neglecting diffusion leads to eq 12.)

These simulations were less stable, and so the maximum ratio of  $\mu_H/\mu_C$  that could be used was 5. Otherwise, the settings were the same as those used in the base case.

The simulated polymer still reduced under these conditions, and this occurred through migration of a front that broadened over time and whose velocity was proportional to the applied voltage, just as in the base case. In addition, the front shapes were similar. The ion and potential profiles and the front position vs time are shown in the Supporting Information (SI section 2.8). (They are not shown here because the ratio  $\mu_H/\mu_C = 5$  makes direct comparison with the base case impossible; these results are more comparable to those in the previous finite hole mobility section.)

The results of this simulation are significant because only the voltage drop over the polymer provided the driving force for reduction. There was no contribution from net charge, yet the results were essentially the same. *The question of whether charge neutrality is or is not strictly enforced everywhere is therefore largely moot, at least as concerns predictions of charge transport behavior.*

## 5. Results 2: Increased Model Complexity

The simplicity of the base case model allowed good demonstrations of how the model parameters (drift, diffusion, voltage, hole mobility, and charge neutrality) affected the simulated behavior. However, this simplified model did not take into account the experimentally observed concentration dependence of the mobility nor did it include the electrolyte, instead assuming that ion transport in the electrolyte was not a rate-limiting process. In this section, the model complexity is increased to take these factors into account with the aim of making more realistic predictions. These cases have been chosen to address fundamental open questions in the field, such as the effect of non-Fickian diffusion, whether diffusion-only can lead to front propagation, and the effect of the electrolyte.

**5.1. Nonconstant Coefficients.** Experimentally, ion transport depends strongly on the state of the polymer matrix,<sup>33</sup> and Otero

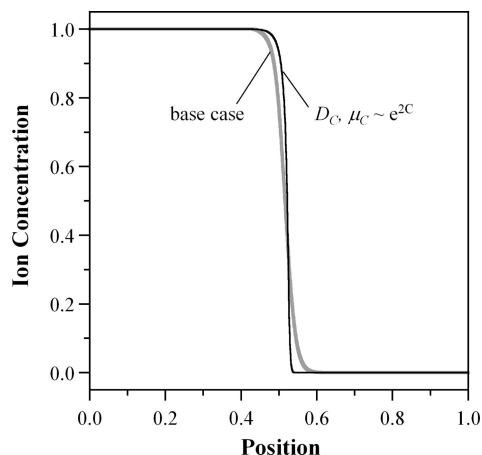


**Figure 14.** Ion concentration profile that results from using concentration-dependent diffusion and migration coefficients at a point when the film is approximately halfway reduced, compared to the base case when the front is in the same position.

et al.<sup>21</sup> have developed a very successful polymer conformational relaxation model to predict peak positions in chronoamperograms that takes the state of the matrix into account. Thus, our model needed to have a mechanism for handling non-Fickian diffusion. One way that non-Fickian diffusion has been dealt with in the literature (albeit with varying degrees of success) has been through a concentration-dependent diffusion coefficient.<sup>34,35</sup> In this section, we explore the consequences of taking this approach.

**5.1.1. Background.** There are numerous models for diffusion of solutes in polymers, as reviewed, for example, by Masaro et al.<sup>36</sup> In most of the models, the diffusion coefficient is of the form  $D = D_0 e^{-\text{something}}$ , where the exponent might be related to the polymer volume fraction, the radius of the diffusing species, a screening parameter, a concentration, a free volume, an activation energy, etc. The model that has been found to be the most applicable to aqueous electrolytes (as opposed to organic species or gases) diffusing in hydrated polymers (as opposed to polymer solutions or gels) is based on work by Yasuda<sup>37</sup> and assumes that diffusion depends on free volume, which has its primary contribution from the water in the polymer

$$D \approx D_0 e^{-(v^* H v_{f,H_2O})} \quad (13)$$

where  $v^*$  depends on the size of the diffusant;  $H$  is the hydration, or volume fraction of water, in the polymer; and  $v_{f,H_2O}$  is the water free volume. This model assumes no interactions between the diffusing species and the polymer and does not take into account temperature effects. A more complex model by Vrentas and Duda does include these effects but has 14 parameters, most of which are unknown.<sup>36</sup> Neither model takes into account increasing polymer volume with penetration of the diffusant. Another free volume model, by Peppas and Reinhart, was designed to apply to cross-linked polymers<sup>36</sup>

$$D = D_0 P_\xi e^{-\frac{kR_h^2}{Q-1}} \quad (14)$$

where  $P_\xi$  is related to the mesh size of the gel;  $k$  is related to the polymer;  $R_h$  is the hydrodynamic radius of the particle; and  $Q$  is the volume degree of swelling. This model also does not take into account interactions between ionized diffusants and the polymer. Models that consider migration have usually assumed the Einstein relation to be valid. There are no models that take into account all of the following factors in PPy(DBS): polymer cross-linking; volume increase upon water and ion

ingress; interactions between ions and polymer, ions and solvent, and solvent and polymer; effective ion size and charge; and chain conformational changes. Masaro et al. concluded that it still remains virtually impossible to estimate or predict the diffusion coefficient for any particular system under specific conditions.

**5.1.2. Approach to Non-Fickian Diffusivity.** It must be emphasized that to properly handle polymer relaxation effects a mechanical model needs to be incorporated into our transport model, which will be the subject of future work. Nevertheless, it is of value to study the incorporation of a rudimentary mechanism to make diffusion non-Fickian.

We based our coefficient dependence on empirical data from ref 4 (Figure 15). We had shown that the front velocity,  $v$ , vs the total charge consumed,  $Q_{\text{tot}}$ , could be reasonably well fit with

$$v \sim e^{2Q_{\text{total}}} \quad (15)$$

but that the front velocity vs the charge associated with strain,  $Q_{\text{strain}}$ , (under Gaussian 1) had a different relationship and was linear

$$v \sim Q_{\text{strain}} \quad (16)$$

On the basis of the data in ref 4, eq 16 is the one that more correctly describes the relationship, but since eq 15 has a stronger dependence on  $Q$  (which is equal to  $C$  in this paper), it will better display any changes in model behavior as a result of making the coefficients nonconstant. Therefore, this was the relationship used here. Assuming the usual proportionality of the ion velocity to the electric field strength and the mobility,  $v = \mu E$ , and assuming that the electronic charge is equal to the number of cations exchanged, we can write the mobility in the form

$$\mu_c = \mu_0 e^{2C} \quad (17)$$

Maintaining the link between diffusivity and mobility that was imposed in the base case,  $D/\mu = 0.026$ , gives the diffusivity the same dependence as the mobility

$$D_C = D_0 e^{2C} \quad (18)$$

This form for the coefficients is analogous to eqs 13 and 14. The PDE for holes was left unaltered (since hole transport is not the rate-limiting step and also because its dependence on  $C$  is unknown), and no other changes were made to eq 9. We ran two scenarios. In the first, drift was included, and in the second, only diffusion was considered. The former was expected to give results that agreed more closely with our experiments than the base case with constant coefficients.

**5.1.3. Diffusion and Migration.** Figure 14 shows the ion concentration profile that results from using the nonconstant coefficients in eqs 17 and 18. Using a concentration-dependent diffusivity and mobility created a sharper front than did the base case. (In fact, this front strongly resembles “same” and “lower” in Figure 11a since in this case the coefficients again depend on  $C$ .) The front position and broadening still propagate with  $\sqrt{t}$  but with an artificially higher velocity because of the larger magnitude of the coefficients (they were not normalized as in Figure 11). (In the figure, the ion concentration profile of the base case was taken when  $t = 0.12$ , while that of the new case was taken at  $t = 0.02$ .)

These differences between the curves were smaller than expected and do not account for discrepancies between the model predictions and experimental data. This addition to the model is therefore not critical if charge transport is dominated

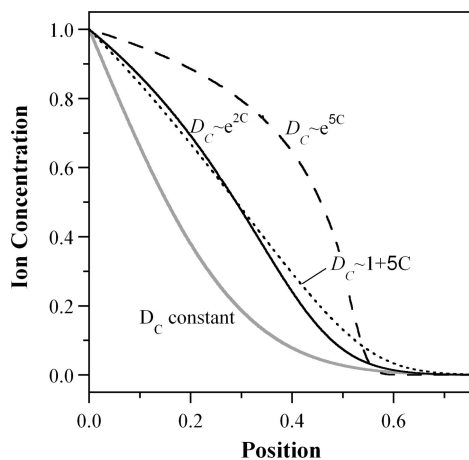


**Figure 15.** Ion concentration profiles resulting from three concentration-dependent ion diffusivities when ion transport is solely by diffusion during reduction. The diffusion-only case with constant coefficients is shown for comparison (gray line).

by migration. We include it, however, in all the sections that follow, unless otherwise noted, because we know with certainty from experimental results that diffusion in these systems is not Fickian. Nevertheless, we can conclude that this method of handling non-Fickian diffusion is unsuitable for PPy(DBS) and probably for other conjugated polymers as well.

**5.1.4. Diffusion Only.** In a second case run with nonconstant coefficients, the migration term in eq 9b was removed so that the ion transport PDE had only a diffusion term. The motivation for simulating this case was to determine the form of the dependence of  $D_C$  on  $C$  that would be needed to produce a front in the absence of migration. Lacroix et al.<sup>5</sup> had previously shown that a hole diffusivity  $D_H$  that increased steeply with the concentration of oxidized sites could lead to a moving front, and for completeness we now did this for ion diffusivity. Furthermore, this case is of interest because a number of theories have assumed that charge moves only due to diffusion. Finally, it is of interest to see whether the experimental results could arise due to ESCR effects (handled here indirectly through the concentration-dependent diffusion coefficient) combined with transport solely by ion diffusion. Once again, only the diffusivity of the ions was made concentration dependent, and the PDE for holes was left unaltered.

Figure 15 shows ion concentration profiles for three relationships between diffusivity and ion concentration: a linear relationship (as in eq 16)

$$D_C = D_0(1 + 5C) \quad (19)$$

the exponential relationship in eq 18, and an even steeper exponential relationship

$$D_C = D_0 e^{5C} \quad (20)$$

The linear relationship was designed to have the same diffusivity as eq 18 at an ion concentration of 1.

The linear relationship, unsurprisingly, produces no front in the event that transport is by diffusion alone. The experimental relationship  $D_C \sim e^{2C}$ , however, results in a curve with an inflection point, which is thus quasi-frontlike. The very steep exponential relationship of eq 20 produces even more of a frontlike shape, and its position advances with the square root of time. However, since there is no migration in this model, the front velocity is independent of the voltage and so does not

match the experimental results. This lack of a dependence on  $V$  arises because the electrolyte is not yet included in the model.

Of these curves, it is actually the base case, with  $D_C = \text{constant}$ , and the linear case that most closely resemble the experimental color profiles at low voltage (compare Figure 7 in ref 4). This may indicate that the linear dependence on  $C$  is more appropriate than the exponential, consistent with the charge associated with strain rather than the total charge. Alternatively, it may indicate that the form of the diffusion term in the model is fundamentally incorrect. Rather, a different method of handling the non-Fickian diffusion may be needed to correctly model transport at low  $V$ , such as including chain conformational changes, elastic energies, or changes in modulus with doping.

**5.2. Addition of the Electrolyte.** The next step in increasing model complexity was to add ion transport within the electrolyte, retaining the nonconstant coefficients. With this addition, the model was as complete as it could be made based only on charge transport PDEs and the Poisson equation. We therefore refer to this as the “full model” and use it in later papers to examine how changes in the polymer or the experimental configuration change the ion transport behavior.

In the model up to this point, the same voltage drop was imposed across the polymer throughout the reduction process, regardless of whether it was oxidized, and thus highly conductive, or reduced and highly resistive. In reality, however, the potential is instead dropped across the electrolyte when the polymer is conductive. Considering the polymer and the electrolyte as if they behave as two resistors in series, the potential across the polymer (which has a variable resistance) depends on the magnitude of its resistance versus that of the electrolyte through a simple voltage-divider relation. Thus, this full model was expected to give more accurate predictions of the electric fields in the film, which translates directly to better predictions of ion profiles and front velocities vs time.

Another reason that it was important to add the electrolyte was to examine the effect of ion depletion and ion double-layer buildup at the polymer/electrolyte boundary. It has been postulated that even if ion transport is by diffusion only, a high ion concentration in the double layer may account for the observed faster redox speeds with higher applied voltages (diffusive elastic metal model<sup>38</sup>). This could only be investigated by the addition of the electrolyte.

**5.2.1. Full Model.** The electrolyte was added as a second material, as illustrated in Figure 16. Charge transport in the electrolyte was governed by the following PDEs. These are essentially identical to those used in polymer, but instead of holes, eq 22 accounts for the anions, and the net charge in eq 23 is simply given by the difference between the anion and cation concentrations at a given location. Convection, which is small in unstirred solutions, was not included in the electrolyte model.

$$\frac{\partial C_e}{\partial t} = -\nabla \cdot (-D_{C_e} \nabla C_e - \mu_{C_e} C_e \nabla \phi) \quad (21)$$

$$\frac{\partial A}{\partial t} = -\nabla \cdot (-D_A \nabla A + \mu_A A \nabla \phi) \quad (22)$$

$$\epsilon_0 \nabla \cdot (\epsilon_e \nabla \phi) = Q = C_e - A \quad (23)$$

Here  $C_e$  is the cation concentration in the electrolyte;  $A$  is the anion concentration in the electrolyte;  $D_{C_e}$  is the diffusivity;  $\mu_{C_e}$  is the mobility of the cation in the electrolyte;  $D_A$  is the diffusivity and  $\mu_A$  is the mobility of the anion in the electrolyte; and  $\epsilon_e$  is the dielectric constant of the electrolyte. The ion diffusivity and mobility in the polymer are as given by eqs 17 and 18.

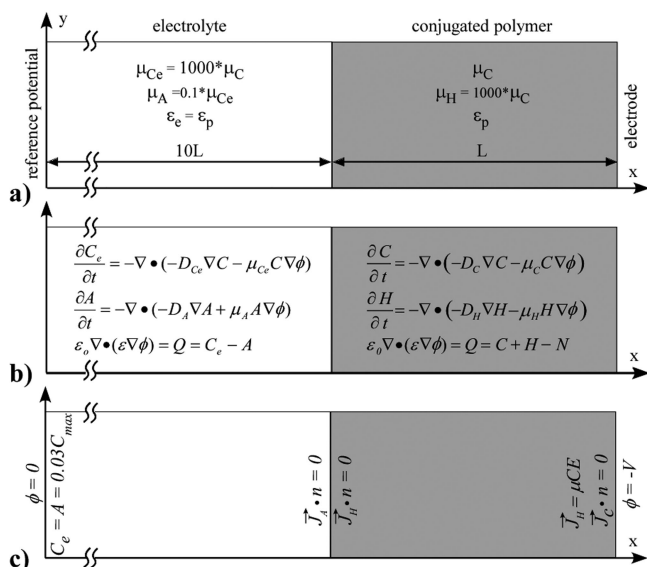


**Figure 16.** (a) Parameters, (b) PDEs, and (c) boundary conditions used during reduction in the full model, a 1-D model that includes the electrolyte and nonconstant coefficients.

As in the previous section, we began with a starting point case. Both anions and cations were treated as singly charged. In the electrolyte, the cations were assumed to have a  $10 \times$  higher mobility than the anions (Figure 16a) since in our experiments the  $\text{Na}^+$  is much smaller than the  $\text{DBS}^-$ . The cation mobility in the electrolyte was assumed to be 1000 times higher than in the polymer, based on reported diffusivity values in the literature.<sup>39,40</sup> The Einstein relation was assumed to be valid, and the dielectric constant of the electrolyte was set to the same value as that for the polymer. The electrolyte was set to be  $10 \times$  longer than the polymer, based on our experimental configuration. The parameters in the polymer were the same as those used in the base case, except for the implementation of nonconstant coefficients.

There were three boundaries in the new model (Figure 16c). On the left-hand side ( $x = -10$ ) is a second electrode, equivalent to an experimental configuration in which the counter and reference electrodes are shorted. At this electrode/electrolyte boundary, the anion and cation concentrations were set equal to the salt concentration in the bulk of the electrolyte. Since we used a 0.1 M electrolyte concentration for the experiments, this was also used in the model system (equal to  $0.033 C_0$ , since  $C_{max} = 3$  M). The potential at that boundary was zero during the reduction process. The interface between the electrolyte and the polymer ( $x = 0$ ) had a no-flux condition for anions and holes, keeping them confined in the electrolyte and polymer, respectively. Lastly, the polymer/electrode interface ( $x = 1$ ) had the same boundary conditions as in the base case.

In the initial conditions for the simulation, anion and cation concentrations throughout the electrolyte were equal to  $0.033 C_0$ . In the polymer, the initial conditions were the same as used in the base case:  $C = 0$  and  $H = 1$ .

**5.2.2. Full Model Results.** The concentrations of the charged species are shown in Figure 17a when the front has reached halfway into the polymer. In the new electrolyte region, both anions and cations are depleted near the surface of the polymer, their concentrations returning to bulk values by  $x = -4$ . Just at the interface, though, the cation concentration rises steeply, forming a thin double-layer (more clearly seen in the inset of Figure 17a). The profiles in the polymer are qualitatively similar to those in the base case.

The electric field (Figure 17b), which is  $\vec{E} = -\nabla \phi = -d\phi/dx$  in this 1-D case, creates a sharp build-up of cations in the electrolyte ( $C_e$ ) at the electrolyte/polymer boundary; i.e., the cations form a double-layer. The reason for this is that the ion migration flux is the product of three terms: ion mobility, ion concentration, and electric field (eq 21). The electric field is nearly zero in the bulk of the electrolyte (on the left), becomes high near the electrolyte/polymer boundary, drops to a low value in the reduced part of the polymer, and returns to almost zero in the conducting region. The ion concentration in the bulk of the electrolyte is  $\sim 30$  times lower than in the reduced polymer, but the mobility is 1000 times larger (see Figure 16 and Figure 17). Thus, the flux in the electrolyte near the polymer ( $\mu_{C_e} C_e E = \text{very high} \times \text{low} \times \text{very high}$ ) is far greater than in the reduced part of the polymer ( $\mu_C C E = \text{low} \times \text{high} \times \text{low}$ ). The faster arrival of cations at the boundary than they can be taken up by the polymer causes the pile-up of ions at the interface. Diffusion, which opposes such concentration gradients, limits the size of this double-layer.

The rapid supply of cations to the electrolyte/polymer boundary further creates a cation depletion region to the left of the boundary, within the region  $-2 < x < -0.1$ , as seen in the inset of Figure 17. The flux in the bulk of the electrolyte, because of the small  $E$  field there, cannot keep up with the supply of ions to the double-layer. There is also a depletion of anions near the interface, caused directly by the electric field, which attracts the cations but repels the anions.

The potential as a function of position is shown at three time snapshots in Figure 17b. Initially, when the polymer is in its conducting, oxidized state, all of the voltage is applied across the electrolyte. As the polymer is reduced, the potential across it rises, but even so, halfway through the reduction process approximately 70% of the potential drop is still across the electrolyte. The largest part of this drop occurs across the depletion and double layer regions. The profile does not change significantly thereafter: at the end of the process, only slightly more of the potential is dropped across the polymer.

The front position moves as  $\sqrt{t}$  in the polymer (shown in the Supporting Information, section 3.3), just as it did in the base case. This is because after an initial rapid increase, up to  $t = 0.01$ , the potential across the polymer grows only slowly. (The potential drop across the polymer over time is shown in SI section 3.2). Therefore, the behavior is, as in the base case, dominated by the change in width of the conducting region as the front moves forward. The front also still broadens as  $\sqrt{t}$ . (This is also shown in the SI, section 3.3.) In addition, the effective front velocity is still linearly proportional to the applied potential. Regardless of the size of the applied voltage, this model did not show a limiting front velocity due to transport in the electrolyte.

The small differences in behavior between this full model and the previous one, in section 5.1, stems from the fact that potential drop across the electrolyte is substantial, particularly across the depletion layer. This lowers the migration term in the polymer. If the potentials across the polymer in the two models are equal, approximated by using a value of  $V = 0.25$  in the base case, the two produce essentially identical results (see SI section 3.3).

**5.2.3. Variation: Diffusion Only.** Because of the continued discussion in the literature maintaining that ion transport is due only to diffusion, this question was examined once again using the full model. In the diffusive elastic metal model,<sup>38</sup> the force for ion transport into the polymer is a high concentration of ions in the double layer at the polymer/electrolyte interface, and

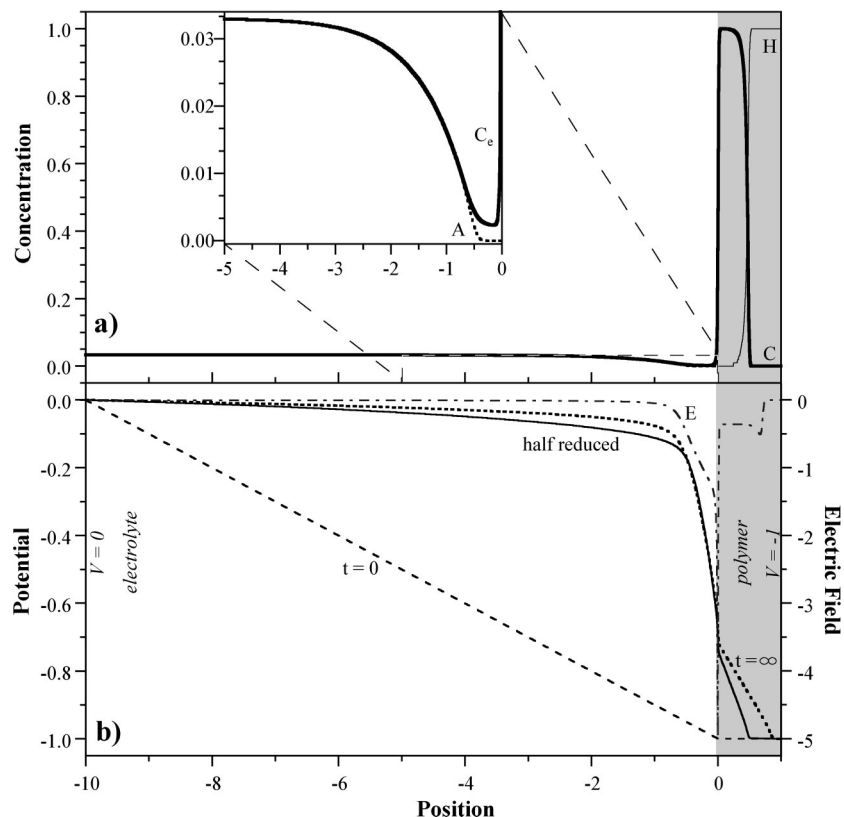


**Figure 17.** Simulation results for reduction using the full model, which includes the electrolyte and nonconstant coefficients. The gray on the right-hand side indicates the location of the polymer. (a) Anion, cation, and hole concentrations as a function of position. The inset shows a close-up of the electrolyte adjacent to the polymer. (b) The potential as a function of position at three different times and the electric field  $E$  (dot-dashed line) when the film is halfway reduced.

diffusion is linked to the applied potential indirectly through changes in the double-layer ion concentration.

Migration was removed in the full model in four different ways, taking away, without any other alterations in the model, (1) the cation migration term in the polymer, (2) the cation and hole migration terms in the polymer, (3) the cation and anion migration terms in the electrolyte, or (4) the migration terms for cations, anions, and holes everywhere. Here, we present the results of the first case because it corresponds directly to the diffusive elastic metal model. Results from the other three cases are given in the Supporting Information (SI section 3.4) since they do not have clear physical meanings.

The consequences of setting the cation migration term in the polymer to zero are shown in Figure 18. For  $t < 2$ , there is quasi-frontlike behavior, in that the concentration at  $x = 1$  does not change immediately (Figure 18a and b) and that the curve has an inflection.

For  $V$  smaller in magnitude than  $-2$ , the polymer does not fully reduce (Figure 18a and c). For  $V$  smaller in magnitude than  $-1$ , the cations reach a maximum value in the polymer equal to their value in the double layer, and the ion concentration eventually reaches this value throughout the film. This result does not correspond to physical reality. (A partially reduced film only occurs experimentally when a voltage below the full reduction potential is applied, but in the models in this paper, a partially reducing potential does not exist.) The final ion concentration in the polymer increases with the applied potential, as shown in Figure 18c, because a more negative reduction potential can pull more ions into the double layer. However, the polymer can only be completely reduced for  $V > 10$ .

At high voltages,  $C$  went to unrealistically large values near the interface at early times (Figure 18b). (Not only have ion

concentrations  $> 1$  not been seen experimentally, but out-of-plane volume measurements have expressly shown that they do not occur at any point during reduction.<sup>33,41</sup>) The high initial concentrations dropped over time, and at the end of the reduction process,  $C \approx 1$  throughout the polymer.

An important question to be answered by this simulation was, "Is the reduction speed voltage-dependent?". As shown in Figure 18d, it was. The speed went as  $0.24 + 0.08 \log(V)$ . This is because, unlike in the base case with diffusion-only (compare section 5.1.4), the concentration at  $x = 0$  is not fixed at 1 but varies with the concentration in the double layer. Using a higher reduction potential increases the ion concentration in the double layer through a stronger migration term in the electrolyte. This occurs even for voltages at which  $C$  stays below 1. This is a demonstration of the ion transport mechanism postulated in the diffusive elastic metal model. However, the facts that the polymer does not fully reduce and that the velocity is logarithmic rather than linear with  $V$  indicate that this case is not physically relevant (it does not account for the totality of the experimental observations).

The results of using a diffusivity proportional to  $e^{5C}$  (eq 20) to force the emergence of a front are shown in SI section 3.4.1. The outcomes are basically the same as those in Figure 18, but the concentration profiles have a more pronounced front. Again, the polymer does not fully reduce below  $\phi \sim 2$ , and the reduction velocity goes as the log of the voltage. As usual, the front propagates with  $\sqrt{t}$  since the charge is driven by only diffusion.

## 6. Summary of Model Development Results

We have simulated a base case model with parameter variations (to understand how the model behaves), cases with

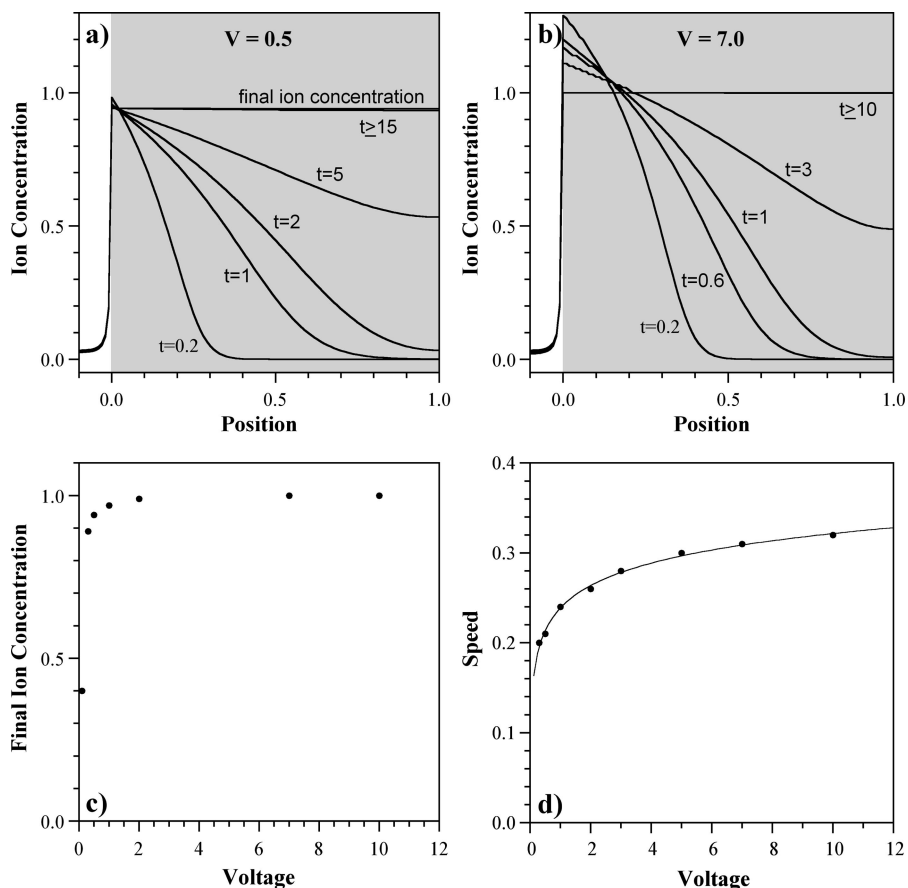


**Figure 18.** Results of the diffusion-only full model during reduction when the migration of ions in the polymer is turned off and  $D_C = D_0 e^2 C$ . Ion concentration profiles for (a)  $V = 0.5$  and (b)  $V = 7$ . The gray on the right side indicates the location of the polymer. (c) Final ion concentration in the polymer under different potentials. (d) Front velocity vs potential. The line shows a log fit.

nonconstant coefficients (to address, for example, the experimental observation that diffusion is not Fickian), and cases in which ion transport is by diffusion only (to address the postulation in the literature that ions do not move in the polymer by migration), and we have presented a full model that includes the effect of the electrolyte. The key findings of each simulation are summarized in Table 2. Unless noted otherwise, the simulation parameters were the same as in the 1-D base case (upper half of the table) or in the full model (lower half of the table).

Our simulations confirm that, as found by Lacroix,<sup>5</sup> charge transport is not properly described solely by diffusion: the existence of electric fields in the polymer must be taken into account. Numerous diffusion-only models were tested, and *none of them* could reproduce the experimentally observed behavior. Specifically, they did not result in a linear dependence of the reduction rate on the applied voltage. Using constant coefficients, i.e., assuming Fickian diffusion, the base case simulation without a migration term was completely insensitive to voltage, and the ions entered without forming a front. If the diffusion coefficient had a large exponential dependence on  $C$ , making the diffusion non-Fickian, then a front was generated, but its speed still did not depend on potential. In the full model, using an exponential dependence of the diffusion coefficient resulted in a voltage-dependent reduction speed as a result of a voltage-dependent cation concentration in the electrolyte double-layer, but the speed went as  $\log(V)$  rather than  $V$ . Furthermore, the polymer was not fully reduced.

Lacroix<sup>5</sup> had also called attention to the contribution played by local violations of charge neutrality (resulting from an

imbalance in the concentration of electrons and ions) to ion transport. Our modeling confirmed that regions with net charge result in potential drops. However, it also showed that even in the absence of net charge, achieved by enforcing absolute charge neutrality throughout the system, essentially the same results were obtained. Therefore, the existence of net charge is unnecessary for explaining the reduction behavior. Even if all net charge is perfectly screened, electric fields still act on the charges, and migration still plays a significant role in reduction.

The modeling results also shed light on the time dependence of the reduction process. A measured square root of time dependence of the current in an experiment should not lead one to conclude that the transport process is due to diffusion. In the base case simulation, the front velocity  $\sim \sqrt{t}$  even when ion transport was dominated by migration. This arises because the insulating region grows wider as the front propagates.

The addition of the electrolyte layer affects the behavior in the simulations in three ways. First, it changes the voltage at the surface of the polymer from a fixed to a variable value that evolves as the relative resistance of the polymer vs the electrolyte changes with doping level. Second, the ion concentration at the electrolyte boundary of the polymer is also changed from a fixed to a variable value through the introduction of a “double-layer”, or spike in ion concentration, which builds up in response to charges on the polymer. Third, it changes the ion flux from the electrolyte to the polymer because of the development of a depletion layer, which arises because of the high concentration of ions pulled into the polymer in comparison with the much lower bulk electrolyte concentration. For the system modeled in this paper, the results were not strongly

TABLE 2: Summary of the Model Development Cases and the Key Findings of Each

section, case	simulation settings	questions posed	key findings
4.1, 1-D Base Case	(1) Constant $D_C, D_H, \mu_C, \mu_H, \varepsilon$ ; (2) $\mu_H = 1000\mu_C$ ; (3) $D_C/\mu_C = D_H/\mu_H = 0.026$ ; (4) $\varepsilon = 10^{-3}$ ; (5) $V = -1$ on electrode	What behaviors are predicted by the simplest possible model?	(1) Charge transport is due primarily to migration. (2) A cation front moves through the film. (3) The front velocity $v_f$ is $\sim\sqrt{t}$ , even though transport is by migration rather than diffusion. (Recall that the experimental velocity is between $v_f \sim \sqrt{t}$ and $t$ .) (4) The front broadens due to diffusion, with front width $w_f \sim\sqrt{t}$ . This model does not correctly predict diffusion behavior seen in experiments. (5) The applied potential is primarily dropped over the reduced (i.e., insulating) region. (6) The strength of the electric field $E$ and the size of the net charge $Q$ decrease over time as the width of the reduced region grows. <i>In summary, migration dominates the behavior, and migration might be confused with diffusion because of its <math>\sqrt{t}</math> time dependence.</i>
4.2, 2-D Base Case	same as previous	Is it valid to perform 1-D simulations, or are 2-D simulations needed?	(1) Virtually the same results are obtained as in the 1-D case. (2) Cations travel along $E$ field lines that are primarily parallel to the surface. <i>1-D simulations are adequate.</i>
4.3.1, 1-D Base Case, vary $V$	vary applied voltage $V$ : $0.001 < V < 10$	What is the voltage dependence of the behavior?	(1) Front velocity is linearly proportional to applied voltage: $v_f \sim V$ . (2) Diffusion makes a significant contribution to the behavior only when $V$ is small. <i>The voltage dependence matches that seen in the experiments.</i>
4.3.2, 1-D Base Case, change $D/\mu$	(1) $D_C \sim C$ (diffusivity depends on $C$ ); (2) $\mu = \mu_0$	What happens if the Einstein relation is not assumed, but $D/\mu$ depends on charge concentration?	(1) Fronts are somewhat sharper than in the base case. (2) Fronts have the same velocity as in the base case at high voltage but are slightly faster at low voltage. <i>It does not make a significant difference if one assumes the Einstein relation or not.</i>
4.3.3, 1-D Base Case, low hole mobility	$\mu_H = \mu_C$	What happens if the holes are <i>not</i> much faster than the ions?	(1) The cation front propagates linearly with time: $v_f \sim t$ . (2) $\phi$ drops linearly across the entire polymer. (3) Front broadening increases. (4) Front velocity decreases. <i>The behavior is dramatically affected if the hole mobility is reduced. This might be one explanation for the experimentally observed range of <math>v_f</math> between <math>\sqrt{t}</math> and <math>t</math>.</i>
4.3.4, 1-D Base Case, charge neutral	(1) $H = 1 - C$ ; (2) $\mu_H = 5\mu_C$	How does the behavior change if charge neutrality is strictly enforced in the polymer (no net charge permitted)?	(1) Essentially the same results as in the base case but reflecting the lower hole mobility that needed to be used to make this simulation run. <i>It makes no real difference whether charge neutrality is enforced.</i>
5.1, base case with nonconstant coefficients	$D_C = D_0e^{2C}, \mu_C = \mu_0e^{2C}$	Increase the model complexity to better reflect the physical system. What changes if diffusion is non-Fickian?	(1) No substantial differences from the base case; the fronts are a little sharper. (2) Front velocity still goes as $v_f \sim\sqrt{t}$ and $v_f \sim V$ . (3) Front width still goes as $w_f \sim\sqrt{t}$ . (4) Front velocities are artificially higher (by a factor $e^{2 \times 0.5} = 2.7$ ), an artifact of the larger magnitudes of the coefficients. (5) At low $V$ , the concentration profiles still do not resemble the experimental data. <i>Extending the model to introduce non-Fickian diffusion still does not correctly capture the experimentally observed diffusion behavior.</i>
5.1.4, Base Case, diffusion only, nonconstant coefficients	(1) $D_C = D_0(1 + 5C), D_0e^{2C}$ , or $D_0e^{5C}$ ; (2) $\mu_C = 0$	If cation diffusion is non-Fickian, can a front be formed if the ions move only by diffusion?	(1) For $D_0e^{2C}$ , there is quasi-frontlike behavior, and for $D_0e^{5C}$ , a real front is formed. (2) The front velocity still goes as $v_f \sim\sqrt{t}$ . (3) Voltage has no effect on the reduction speed. <i>A front can be formed in the film if the ions move only by diffusion if the exponent is large enough, but this model does not correctly predict other experimental behaviors.</i>

**TABLE 2: Continued**

section, case	simulation settings	questions posed	key findings
5.2.2, Full Model	(1) $D_C = D_0 e^{2C}$ , $\mu_C = \mu_0 e^{2C}$ ; (2) New anion, cation PDEs in an electrolyte layer; (3) New boundary conditions, including $\phi = 0$ at the edge of the electrolyte	Increase the model complexity to better reflect the physical system. How is the behavior affected by including the potential drops and ion transport in the electrolyte?	(1) There is a significant voltage drop across the electrolyte. At the end of the reduction process, only ~30% of the voltage drop is across the insulating polymer. (2) Depletion and double layers form in the electrolyte. (3) Front velocity still goes as $v_f \sim \sqrt{t}$ and $v_f \sim V$ . (4) If we set $V = 0.25$ across the polymer in the base case (thereby mimicking a 75% voltage drop across the electrolyte), the resulting charge profiles and front velocity are virtually identical to those in the full model. <i>Under these conditions, the behavior upon including the electrolyte is the same as in the base case after taking into account the resistive potential drop over the electrolyte.</i>
5.2.3, Full Model, diffusion only	(1) $D_C = D_0 e^{2C}$ ; (2) $\mu_C = 0$	How is non-Fickian diffusion-only cation transport affected by the inclusion of an electrolyte layer?	(1) The cation concentration in the polymer equals the cation concentration in the electrolyte double-layer. (2) The polymer does not fully reduce unless extreme voltages are applied ( $V \geq 10$ ). (3) Quasi-frontlike behavior is again seen. (4) The reduction speed does depend on voltage, but the dependence is weak, going as $\log(V)$ . <i>A diffusion-only model does not correctly predict the experimental behavior.</i>

affected by these alterations or, as mentioned previously, by the use of nonconstant coefficients. In fact, the only significant difference arose during the diffusion-only case, where the base case model showed no dependence of the reduction speed on applied voltage, and because of the introduction of the double-layer, the full model did. Thus, it is not necessary to use anything more elaborate than the base case model to describe reduction of covered films of PPy(DBS).

Nevertheless, we shall use the full model in subsequent papers both because it incorporates more realistic physics and because it turns out to be necessary for other geometries, materials, and conditions, such as encountered when examining the effect of electrolyte concentration. In fact, we show in the next paper that inclusion of the electrolyte can dramatically change the predicted behavior and is necessary for understanding thin films.

## 7. Discussion and Conclusions

The contributions of this study were choosing equations, boundary conditions, and numerical methods that were consistent with the known physics and thereby obtaining results that were consistent with experimental measurements. This first-principles approach allowed us to address a broad range of issues (effects of parameter variations, diffusion that is not Fickian, transport by diffusion only, the effect of the electrolyte).

The technical details of the system made the simulations challenging. We took advantage of the full suite of modeling tricks: we used symmetry to reduce model complexity, introduced scaling to handle disparities in dimension (e.g., 1:500 aspect ratios in film thickness to width), used limiting behavior

to disregard some parameters (e.g., too large dielectric constants), rounded corners (e.g., in the film, in ion concentrations) to avoid singularities; meshed more tightly in regions of rapid change, etc.

Given the simplicity of the charge transport model presented in this paper, it did remarkably well in predicting the reduction process in PPy(DBS). It has thus allowed us to answer several important questions that have long been debated in the literature. The first question was, does migration contribute to ion transport in conjugated polymers? This question is fundamental since it involves the basic driving mechanism in devices and thus impacts how they can be controlled. The results unambiguously show that migration must be included since none of the many diffusion-only models that were examined could account for the experimental observations. The behavior switches from diffusion-dominated at small overpotentials to migration-dominated at higher voltages. In the latter cases, the behavior is determined largely by where the voltage drops occur in the system. A second question was, is there a net charge in the polymer? The simulations show that this question is basically irrelevant: the presence or absence of a net charge makes no real difference to the results.

The model also revealed some surprises, such as that migration can lead to  $\sqrt{t}$  time dependences. Previously, experimental results with this time dependence were automatically attributed to diffusion, regardless of the fact that diffusion should not have been expected to be Fickian in these systems.

The model did not account for all of the results, however: it failed to correctly predict the front broadening behavior despite

the fact that the diffusion was treated using an accepted approach for modeling non-Fickian diffusion. We conclude that to do this future models need to include polymeric and/or electrochemical contributions to the transport.

**Acknowledgment.** We would like to acknowledge the Laboratory for Physical Sciences and the Dupont Young Professor Award for supporting this work. We thank the Comsol technical staff for helping us to solve several simulation issues. We also thank Kevin Lewy, Mario Urdaneta, Jason West, and Pramod Mathai for assistance with our simulation server.

**Supporting Information Available:** Includes additional simulation results, including more detailed derivations, the effects of varying parameters such as the dielectric constant, and further charge-neutrality and diffusion-only cases. This material is available free of charge via the Internet at <http://pubs.acs.org>.

## References and Notes

- (1) Albery, W. J.; Mount, A. R. Transmission-line model for conducting polymers including cations and Donnan exclusion. *J. Chem. Soc., Faraday Trans.* **1993**, 89 (14), 2487–2497.
- (2) Fletcher, S. Contribution to the theory of conducting-polymer electrodes in electrolyte solutions. *J. Chem. Soc., Faraday Trans.* **1993**, 89 (2), 311–320.
- (3) Wang, X.; Smela, E. Color and volume change in PPy(DBS). *J. Phys. Chem. C* **2009**, 113, 359–368.
- (4) Wang, X.; Smela, E. Experimental studies of ion transport in PPy(DBS). *J. Phys. Chem. C* **2009**, 113, 369–381.
- (5) Lacroix, J. C.; Fraoua, K.; Lacaze, P. C. Moving front phenomena in the switching of conductive polymers. *J. Electroanal. Chem.* **1998**, 444 (1), 83–93.
- (6) Berthier, F.; Diard, J.-P.; Montella, C. Numerical solution of coupled systems of ordinary and partial differential equations. Application to the study of electrochemical insertion reactions by linear sweep voltammetry. *J. Electroanal. Chem.* **2001**, 502, 126–131.
- (7) Deiss, E.; Haas, O.; Schlenoff, J. B. Numerical-simulation of the cyclic voltammogram of polyacetylene. *J. Electrochem. Soc.* **1995**, 142 (10), 3256–3262.
- (8) Bisquert, J.; Vikhrenko, V. S. Analysis of the kinetics of ion intercalation. Two state model describing the coupling of solid state ion diffusion and ion binding processes. *Electrochim. Acta* **2002**, 47 (24), 3977–3988.
- (9) Wang, X.; Shapiro, B.; Smela, E. Visualizing ion transport in conjugated polymers. *Adv. Mater.* **2004**, 16 (18), 1605–1609.
- (10) Wang, X.; Shapiro, B.; Smela, E. Modeling charge transport in conjugated polymers; SPIE 13th Annual Int'l. Symposium on Smart Structures and Materials, EAPAD, San Diego, CA, 2006.
- (11) Bard, A. J.; Faulkner, L. R. *Electrochemical Methods: Fundamentals and Applications*, 2nd ed.; John Wiley & Sons, Inc.: New York, 2001.
- (12) Bay, L.; Jacobsen, T.; Skaarup, S.; West, K. Mechanism of actuation in conducting polymers: osmotic expansion. *J. Phys. Chem. B* **2001**, 105 (36), 8492–8497.
- (13) Streetman, B. G.; Banerjee, S. *Solid State Electronic Devices*, 5th ed.; Prentice-Hall: Upper Saddle River, 2000.
- (14) Smela, E. Microfabrication of PPy microactuators and other conjugated polymer devices. *J. Micromech. Microeng.* **1999**, 9, 1–18.
- (15) Schey, H. M. *Div, Grad, Curl, and All That: An Informal Text on Vector Calculus*; W. W. Norton & Company: New York, 1973.
- (16) Ashcroft, N. W.; Mermin, N. D. *Solid State Physics*; Saunders College: Philadelphia, 1976.
- (17) Guidoni, S. E.; Aldao, C. M. On diffusion, drift and the Einstein relation. *Eur. J. Phys* **2002**, 23, 395–402.
- (18) Feynman, R. P.; Leighton, R. B.; Sands, M. *The Feynman Lectures on Physics*; Addison-Wesley Publishing Company, 1964.
- (19) Roichman, Y.; Tessler, N. Generalized Einstein relation for disordered semiconductors—implications for device performance. *Appl. Phys. Lett.* **2002**, 80 (11), 1948–1950.
- (20) Panton, R. L. *Incompressible Flow*, 2nd ed.; John Wiley & Sons, Inc.: New York, NY, 1996.
- (21) Otero, T. F.; Boyano, I. Comparative study of conducting polymers by the ESCR model. *J. Phys. Chem. B* **2003**, 107 (28), 6730–6738.
- (22) Singh, R.; Tandon, R. P.; Panwar, V. S.; Chandra, S. Low-frequency AC conduction in lightly doped polypyrrole films. *J. Appl. Phys.* **1991**, 69 (4), 2504–2511.
- (23) Wessling, B. In *Handbook of Conducting Polymers*, 2nd ed.; Skotheim, T. A., Elsenbaumer, R. L., Reynolds, J. R., Eds.; Marcel Dekker, Inc.: New York, 1998; pp 467–530.
- (24) Pironneau, O. *The Finite Element Methods for Fluids*; John Wiley and Sons: New York NY, 1989.
- (25) John, R.; Wallace, G. G. Doping-dedoping of polypyrrole: a study using current-measuring and resistance-measuring techniques. *J. Electroanal. Chem.* **1993**, 354, 145–161.
- (26) Geniès, E. M.; Bidan, G.; Diaz, A. Spectroelectrochemical study of polypyrrole films. *J. Electroanal. Chem.* **1983**, 149, 101–113.
- (27) Osaka, T.; Naoi, K.; Ogano, S.; Nakamura, S. Dependence of film thickness on electrochemical kinetics of polypyrrole and on properties of lithium/polypyrrole battery. *J. Electrochem. Soc.* **1987**, 134 (9), 2096–2102.
- (28) Kaneto, K.; Ura, S.; Yoshino, K.; Inuishi, Y. "Optical and electrical properties of electrochemically doped n- and p-type polythiophenes". *Jpn. J. Appl. Phys.* **1984**, 23 (3), L189–191.
- (29) Tezuka, Y.; Ohyama, S.; Ishii, T.; Aoki, K. Observation of propagation speed of conductive front in electrochemical doping process of polypyrrole films. *Bull. Chem. Soc. Jpn.* **1991**, 64, 2045–2051.
- (30) Tezuka, Y.; Aoki, K.; Ishii, T. Alternation of conducting zone from propagation-control to diffusion-control at polythiophene films by solvent substitution. *Electrochim. Acta* **1999**, 44, 1871–1877.
- (31) Johansson, T.; Persson, N. K.; Inganas, O. Moving redox fronts in conjugated polymers studies from lateral electrochemistry in polythiophenes. *J. Electrochem. Soc.* **2004**, 151 (4), E119–E124.
- (32) West, K.; Bay, L.; Nielsen, M. M.; Velmurugu, Y.; Skaarup, S. Electronic conductivity of polypyrrole-dodecyl benzene sulfonate complexes. *J. Phys. Chem. B* **2004**, 108 (39), 15001–15008.
- (33) Wang, X.; Smela, E. Ion transport in conjugated polymers: Part I. Experimental studies on PPy(DBS). **2007**, in preparation.
- (34) Schlotter, N. E.; Furlan, P. Y. A review of small molecule diffusion in polyolefins. *Polymer* **1992**, 33 (16), 3323–3342.
- (35) Edwards, D. A. Non-Fickian diffusion in thin polymer films. *J. Polym. Sci., Part B* **1996**, 34, 981–997.
- (36) Masaro, L.; Zhu, X. X. Physical models of diffusion for polymer solutions, gels and solids. *Prog. Polym. Sci.* **1999**, 24, 731–775.
- (37) Yasuda, H.; Lamaze, C. E.; Ikenberr, Ld. Permeability of solutes through hydrated polymer membranes Part I. Diffusion of sodium chloride. *Makromol. Chem.* **1968**, 118, 19–35.
- (38) Madden, P. G. A.; Madden, J. D. W.; Anquetil, P. A.; Vandesteeg, N. A.; Hunter, I. W. The relation of conducting polymer actuator material properties to performance. *IEEE J. Ocean Eng.* **2004**, 29 (3), 696–705.
- (39) Burgmayer, P.; Murray, R. W. Ion gate electrodes. Polypyrrole as a switchable ion conductor membrane. *J. Phys. Chem.* **1984**, 88, 2515–2521.
- (40) Ariza, M. J.; Otero, T. F. Ionic diffusion across oxidized polypyrrole membranes and during oxidation of the free-standing film. *Colloid Surf. A* **2005**, 270, 226–231.
- (41) Smela, E.; Gadegaard, N. Surprising volume change in PPy(DBS): an atomic force microscopy study. *Adv. Mater.* **1999**, 11 (11), 953–957.

# Supporting Information

The order of the sections below follows the order of material presented in the paper. The corresponding sections are indicated.

## 1 Modeling and Theoretical Analysis

### 1.1 Derivation of Non-Dimensional PDEs (for section 3.1.3, Reducing Model Complexity)

This section shows in more detail the derivation of non-dimensional PDEs. After introducing the characteristic length scale, the non-dimensional transport equations become:

$$(24) \quad \begin{aligned} \frac{\partial C}{\partial t} &= -\nabla \cdot \left( -\frac{D_C t_0}{L^2} \nabla C - \frac{\mu_C V t_0}{L^2} C \nabla \phi \right) \\ \frac{\partial H}{\partial t} &= -\nabla \cdot \left( -\frac{D_H t_0}{L^2} \nabla H - \frac{\mu_H V t_0}{L^2} H \nabla \phi \right). \\ \nabla \left( \frac{\varepsilon V}{L^2 z C_0} \nabla \phi \right) &= C + H - 1 \end{aligned}$$

By selecting  $t_0 = L^2 / (\mu_C V)$ , the non-dimensional ion mobility becomes unity, transforming the PDEs to:

$$(25) \quad \begin{aligned} \frac{\partial C}{\partial t} &= -\nabla \cdot \left( -D_C \nabla C - C \nabla \phi \right) \\ \frac{\partial H}{\partial t} &= -\nabla \cdot \left( -D_H \nabla H - \mu_H H \nabla \phi \right) \\ \nabla (\varepsilon \nabla \phi) &= Q = C + H - 1 \end{aligned}$$

$D_C$  is given by the ratio between dimensional diffusion  $\mathbf{D}_C$  and drift magnitude  $\mu_C V$ ,

$D_C = \mathbf{D}_C / \mu_C V$ .  $\mathbf{D}_C$  has units of  $\text{m}^2/\text{s}$ ,  $\mu_C$  has units of  $\text{m}^2/\text{Vs}$ , and  $V$  has units of V. Hence,  $D_C$

is non-dimensional. The hole diffusion coefficient is scaled the same way,  $D_H = \mathbf{D}_H / \mu_C V$ . The

non-dimensional mobilities are  $\mu_C = 1$  and  $\mu_H = \mu_H / \mu_C$ . Finally, the non-dimensional

dielectric coefficient  $\varepsilon = \varepsilon V / L_0^2 H_{max}$  is the dimensional coefficient  $\varepsilon$  normalized by the

characteristic gradient of the electric field  $|\bar{\mathbf{E}}| / L_0 \sim (V / L_0) / L_0$  divided by the maximum charge

concentration  $H_{max}$ .

## 1.2 Derivation of Governing Equations with Enforced Charge Neutrality (for section 4.3.4, Charge Neutrality Strictly Enforced)

Consider the governing equations (9) in the main text. Adding together equations (9)a and (9) b gives

$$(26) \quad \frac{\partial(C + H)}{\partial t} = -\nabla \bullet [(-D_C \nabla C - \mu_C C \nabla \phi) + (-D_H \nabla H - \mu_H H \nabla \phi)].$$

To enforce charge neutrality, we set  $\varepsilon = 0$  in (9)c which forces net charge  $Q = C + H - 1 = 0$ .

This sets the left hand side of (26) to zero since  $C + H = 1$  is constant. So now

$$(27) \quad \begin{aligned} 0 &= -\nabla \bullet [(-D_C \nabla C - \mu_C C \nabla \phi) + (-D_H \nabla H - \mu_H H \nabla \phi)] \\ &= -\nabla \bullet [(-D_C \nabla C - \mu_C C \nabla \phi) + (D_H \nabla C - \mu_H H \nabla \phi)] \\ &= -\nabla \bullet [(-D_C + D_H) \nabla C - (\mu_C C + \mu_H H) \nabla \phi] \end{aligned}$$

where we have used  $H = 1 - C$  to substitute  $\nabla H = -\nabla C$  (second line). By charge neutrality,

knowing  $C$  immediately provides  $H$ , and this eliminates the need for equation (9)b. Both

equation (9)a and (26) contain an ion diffusion term, and the two terms conflict. (This is because

we are forcing ions and holes to exactly track each other, and equation (26) contains a hole diffusion coefficient that is different from the ion diffusion coefficient). We therefore discard the ion diffusion term in (26) to get  $0 = -\nabla \cdot [(\mu_C C + \mu_H H) \nabla \phi]$ , which is equation (12). Equation (12) replaces equations (9)b and c in the charge neutral case, and (12) gives the conductivity of the polymer as it depends on ion and hole mobilities and concentrations. This series of substitutions is equivalent to simply using a drift equation to determine the behavior.

### 1.3 Scaling Factor for Time between the 1D and 2D Simulations (for section 4.2, 2-D Confirmation of 1-D Results)

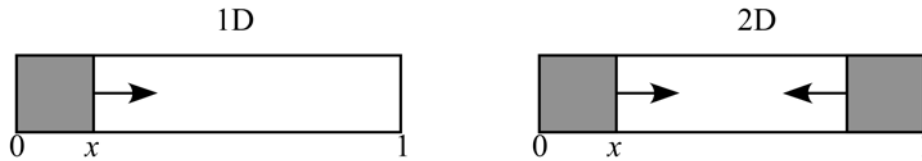


**Figure SM 1. Reduced areas in the 1D and 2D geometries. The 2D geometry has 2 fronts.**

**Therefore, when the front reaches the same position along  $x$ , the reduced area in the 2D geometry is twice as large.**

This section shows the derivation of the scale factor for time between the 1D and 2D simulations. Results are compared when the film reaches the same doping level, which is approximately determined by the front position.

If the front reaches a position  $x_l$  in the 1D simulation, we must compare the results to those at  $x_l/2$  in the 2D simulation (Figure SM 1). In both the 1D and 2D simulations, the fronts propagate with the square root of time. Based on the analysis of front propagation in section 4.1 of the main text, the front position is given by  $x = \sqrt{2\mu_C V} \sqrt{t}$ . The front reaches  $x_l$  in the 1D

simulation at time  $t_1 = (x_1 / \sqrt{2\mu_c V})^2$ . In the 2D simulation, the front reaches  $x_1/2$  at  $t_2 = [(x_1/2) / \sqrt{2\mu_c V}]^2$ . The ratio between  $t_1$  and  $t_2$  is thus  $t_2 = t_1/4$ . The scaling factor is unaffected by the constants used in the non-dimensionalization.

## 2 Base Case Simulation

### 2.1 Variation of Dielectric Constant (for section Error! Reference source not found., Error!

Reference source not found.)

This section demonstrates that using a non-dimensional dielectric constant  $\varepsilon$  of 0.001, which is 8 orders of magnitude larger than the actual value ( $10^{-11} \sim 10^{-8}$ ), does not affect the front propagation results during reduction. The actual value cannot be used in the simulation because it is so much smaller than the other variables, which are close to 1: that would require mesh densities that cannot be handled, due to limitations in computer memory.

To demonstrate that  $\varepsilon$  reaches a limiting value, the simulation was run with 4 different dielectric constants: 0.1, 0.01, 0.001, and 0.0001. The results converged, as shown in Figure SM 2, for  $\varepsilon < 0.001$  (results for 0.001 and 0.0001 overlapped).

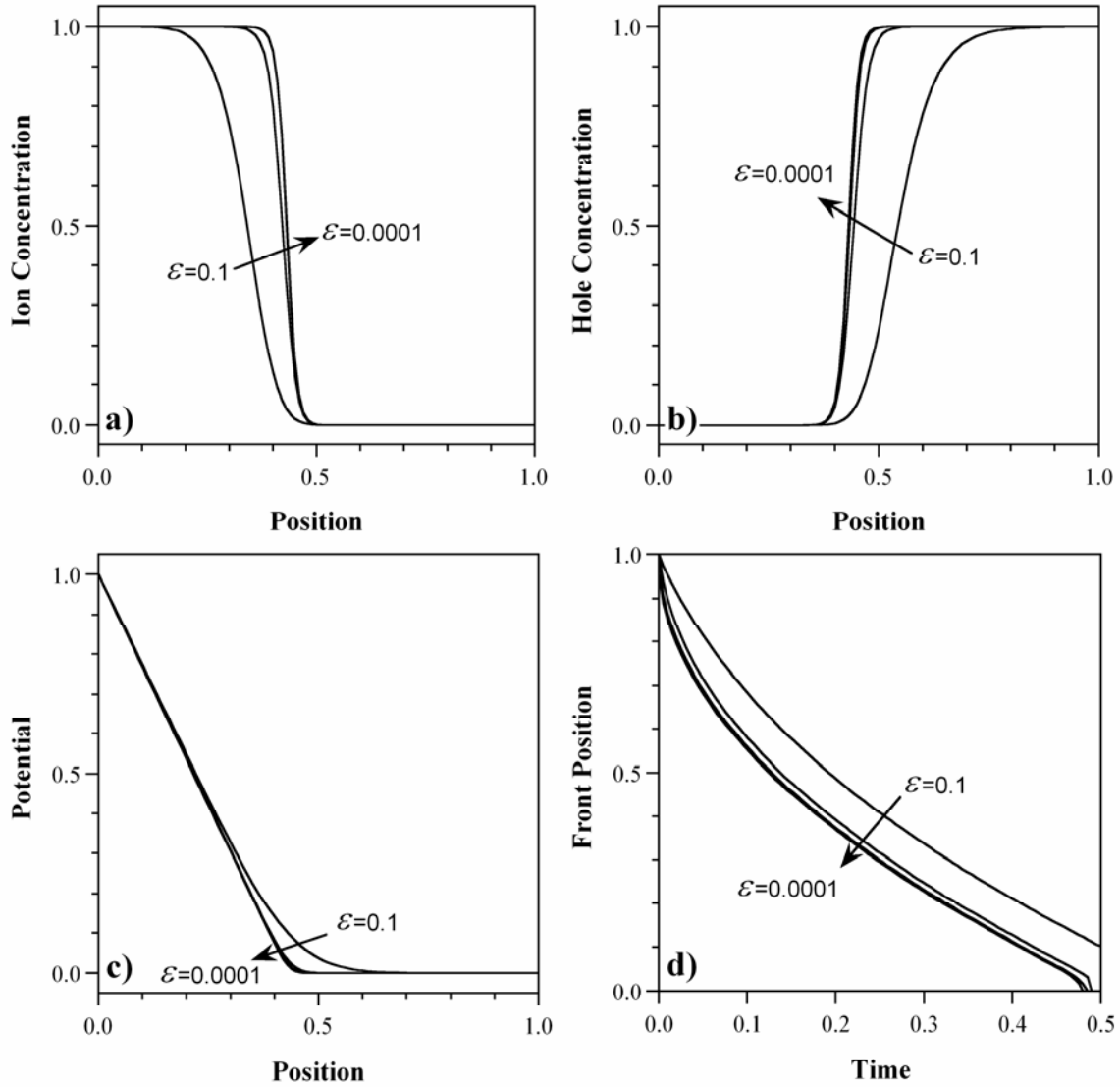


**Figure SM 2. Convergence of simulation results using different  $\varepsilon$  for a) ion concentration, b) hole concentration, c) potential, and d) front position. When  $\varepsilon$  is smaller than 1E-3, the simulation results are identical.**

## **2.2 Comparing Current and Previous Models (for section 4.1, Base Case Simulation Results)**

In previous reports [8,30], in order to reduce model complexity we used an analytical expression for hole concentration instead of the hole transport equation. This is possible under the

assumption that hole transport occurs much faster than ion transport, since in that case the hole concentration can be linked to the potential. Here we compare the ion concentrations in the base case model with those in that prior model (Figure SM 3) and find that they are identical.

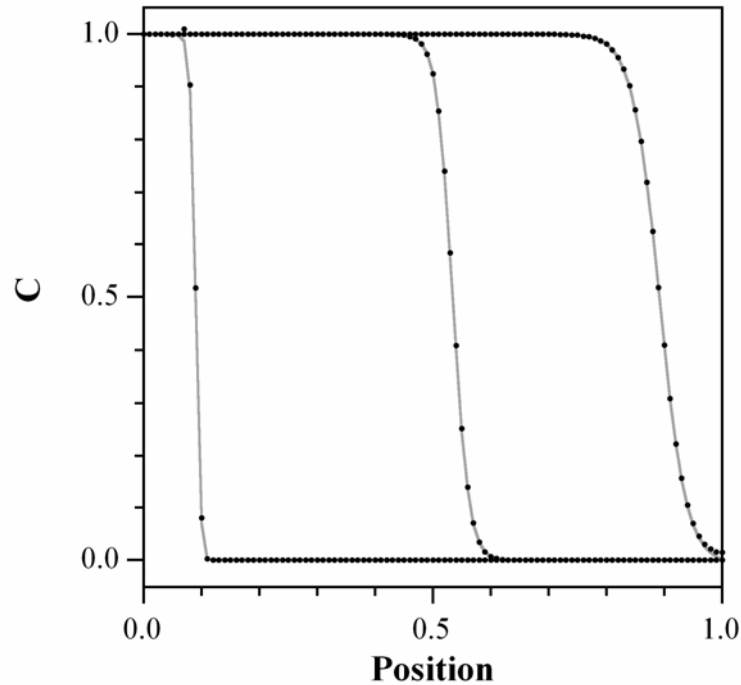


**Figure SM 3. Comparison of the ion concentration profiles obtained by solving the three PDEs of equation (9) (gray line) with those obtained using an analytical solution for the holes (points).**

One might ask, what is advantage of the current model, if the results are identical? The 3<sup>rd</sup> PDE allows us to study a wider range of cases: cases in which  $\mu_H$  is not  $\gg \mu_C$ , in which non-constant coefficients are used, and in which the model is used to predict oxidation.

### 2.3 Net Charge and Front Broadening at Different Reduction Potentials (for section 4.3.1, Voltage)

Figure SM 4 shows the net charge in the film under higher ( $V = 1.5$ ) and much lower ( $V = 0.001$ ) reduction potentials than in the base case ( $V = 1$ ). At very low potential, the film is basically charge-neutral everywhere. With increasing reduction potential, the net charge at the front increases, and its distribution narrows.

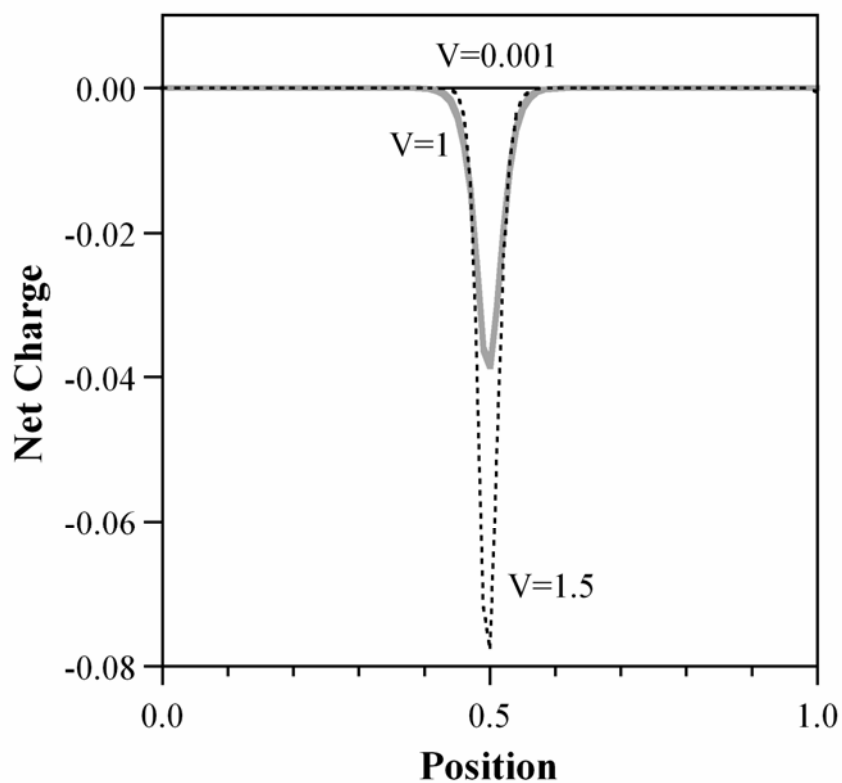


**Figure SM 4. Net charge in the polymer for different reduction potentials when the polymer is approximately half-way reduced.**

The *effective broadening velocity* was determined from the width of the front at time  $t = 0.1$ .

This is plotted in Figure SM 5 as a function of the applied potential. The broadening decreases approximately as  $1/\sqrt{V}$ .

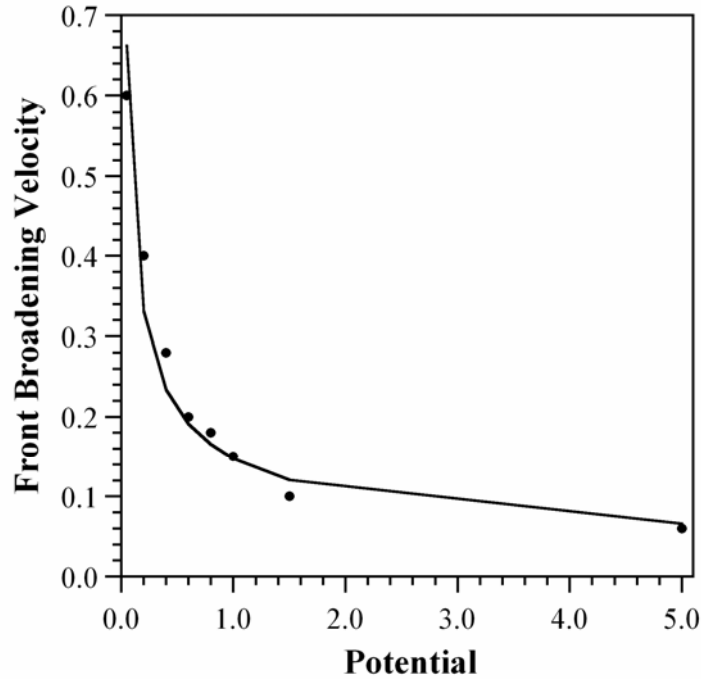
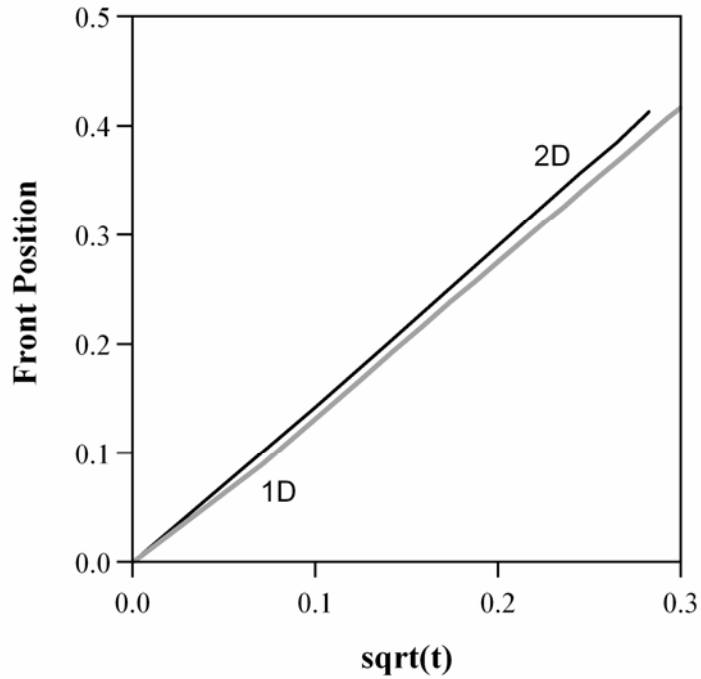


Figure SM 5. Effective front broadening velocity (width at  $t = 0.1$ ) vs. potential. The curve is the line  $y = 0.148 \cdot V^{-0.5}$ .

#### 2.4 Front Propagation along the Electric Field Line in the 2-D Base Case (for section 4.2, 2-D Confirmation of 1-D Results)

Figure SM 6 compares the front propagation along the electric field line in the 2D simulation with front propagation in the 1D simulation. The front position for the 2D simulation was obtained from the ion concentration profile along the electrical field streamline at  $y = 0.15$ . The front moves slightly faster in the 2D case.



**Figure SM 6. Front position vs. the square root of time for the 1D and 2D simulations.**

**2.5 Ion Concentration Profiles when Hole Mobility Equals Ion Mobility (for section 4.3.3, Finite Hole Mobility)**

Figure SM 7 shows ion concentration profiles at different times when  $\mu_H = \mu_C$ . Since the potential  $\phi$  drops across the whole polymer (Figure 12), and does not change with time, the migration term in the reduced area is smaller than in the base case. As a result, the concentration profiles are wider.

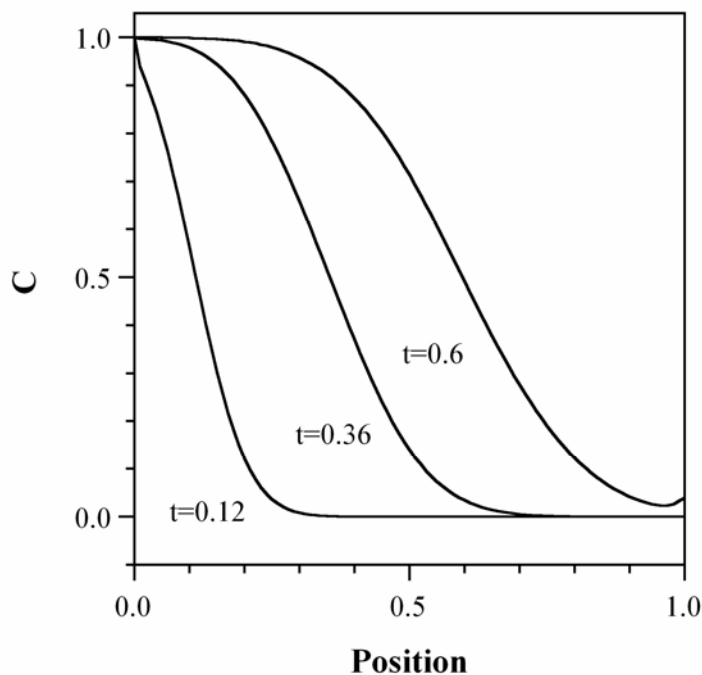


**Figure SM 7. Ion concentration profiles when  $\mu_H = \mu_C$  at three times during reduction.**

**2.6 Effect of Concentration at the Polymer/Electrolyte Interface (for section 3.1.2.2, Boundary and Initial Conditions)**

Figure SM 8 and Figure SM 9 show how the ion concentration at the polymer/electrolyte interface affects the simulation results. The lower concentration value represents the bulk electrolyte concentration (0.03), and the higher value the concentration in the double layer (2.00). The maximum ion concentration in the polymer ( $C = C_0 = 1$ ) used in the base case is shown for comparison.

Within the bulk of the polymer, all three profiles have the same shape: the reduced area has  $C = 1$ , and the oxidized area has  $C = 0$ . However, using a lower concentration results in a slower-

moving front (Figure SM 9). It also has this interesting effect: it makes the front move *linearly* with time.

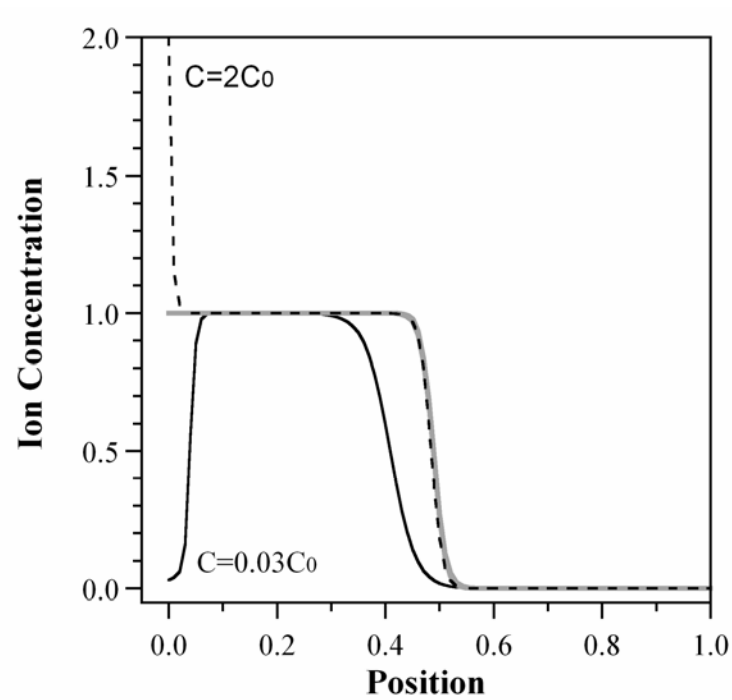


**Figure SM 8.** Ion concentration profiles for different ion concentrations at  $x = 0$ ; the gray line shows the base case, in which  $C|_{x=0} = 1$ .

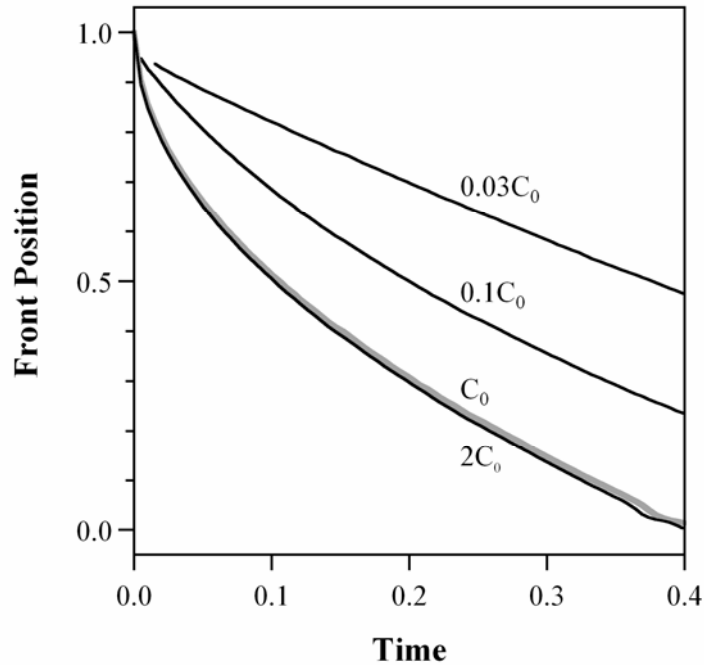


**Figure SM 9. Front propagations when different values are used for different ion concentrations at the polymer/electrolyte interface.**

## **2.7 Base Case Simulation with Only Diffusion for Ions and Holes (for section 4.3.1, Voltage)**

Figure SM 10 shows ion and hole concentrations at different time snapshots when they are both driven by diffusion only. In this simulation, the hole boundary condition at the electrode is set to zero (rather than using the flux boundary condition, which causes the simulation to crash).

While the ion profiles resemble those in Figure 9c, the hole profiles bear no relation to what they should because if ions and holes are driven by diffusion only, their movement becomes uncoupled (charge neutrality cannot be enforced). As a result, this case leads to unphysical results, as is also illustrated by the potential profile (Figure SM 11).

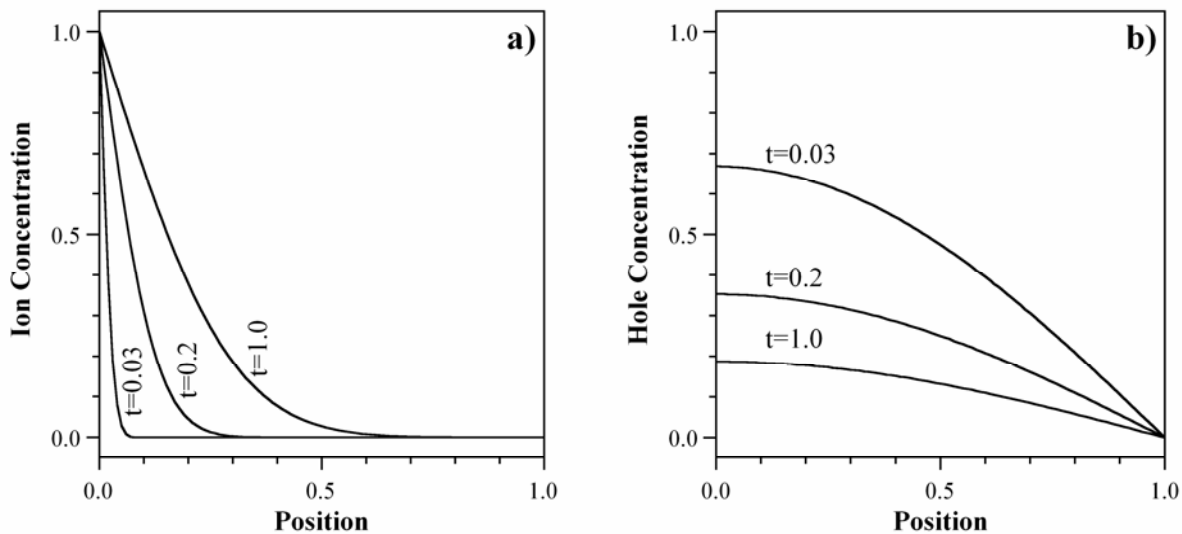


**Figure SM 10. a) Ion concentration profiles at  $t = 0.01, 0.2,$  and  $1.0$  for a simulation in which ions and holes move by diffusion only. b) The corresponding hole concentrations. Since holes have 1000 times higher mobility, they leave the film quickly.**

The ions diffuse into the polymer (Figure SM 10a) because at the electrolyte/polymer boundary,  $C = 1$ . If this were set to another value, then these curves would simply be multiplied in height accordingly, with the final equilibrium value in the polymer equal to the concentration set at the boundary.

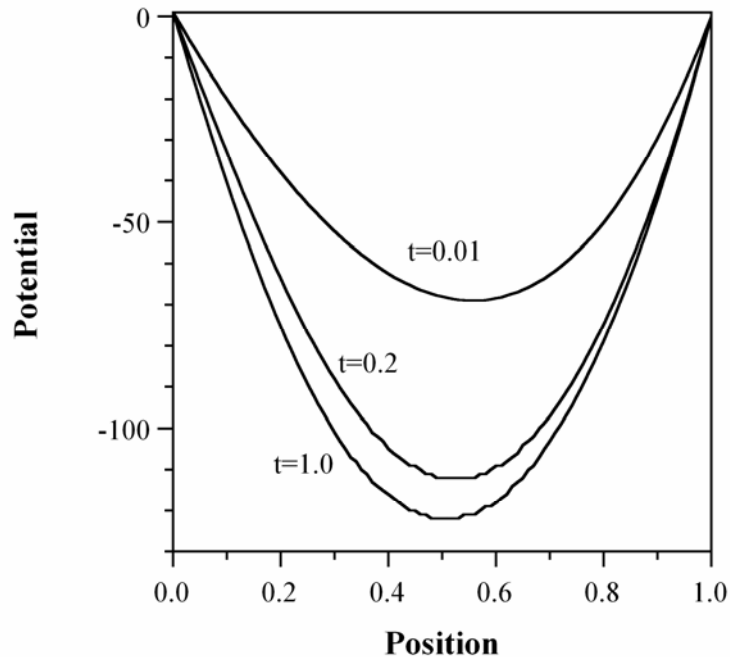


**Figure SM 11. Potential profiles at three times during a simulation in which ions and holes move only by diffusion.**

## **2.8 Base Case with Charge Neutrality Enforced (for section 4.3.4, Charge Neutrality Strictly Enforced)**

Ion concentration profiles at different times from the charge neutrality case are shown in Figure SM 12a. As in the base case, the ions travel into the film at a front, and this front broadens over time. In addition (not shown), once again the speed of the front was proportional to  $V$ .

The potential profile at  $t = 0.25$  is presented in Figure SM 12b. Although the potential drops mainly in the reduced area, since the hole mobility was only 5 times higher than that of the ions, a portion of the potential also drops in the oxidized area. If it were possible to use a higher hole mobility in the simulation, the results would have resembled the base case more closely.

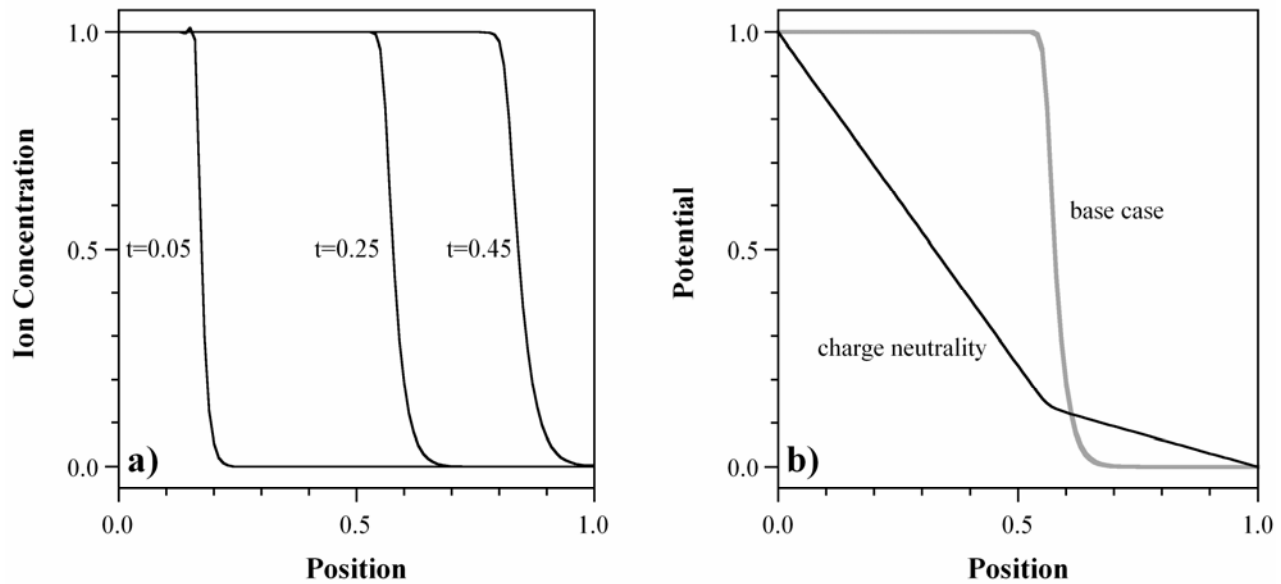


**Figure SM 12. a) Ion concentration profiles at different times when charge neutrality is enforced in the polymer. Note that the hole mobility is only 5 times that of ions (necessary for the simulation to run). b) Potential profiles at  $t = 0.25$  for the charge neutral (black line) and base (gray line) cases.**

The front position vs. time with charge neutrality strictly enforced is shown in Figure SM 13.

Again because  $\mu_H/\mu_C = 5$ , this front moves more slowly (there is a smaller voltage drop across the reduced region) and the velocity is more constant. These results arise from the small hole mobility, not from enforcing charge neutrality.

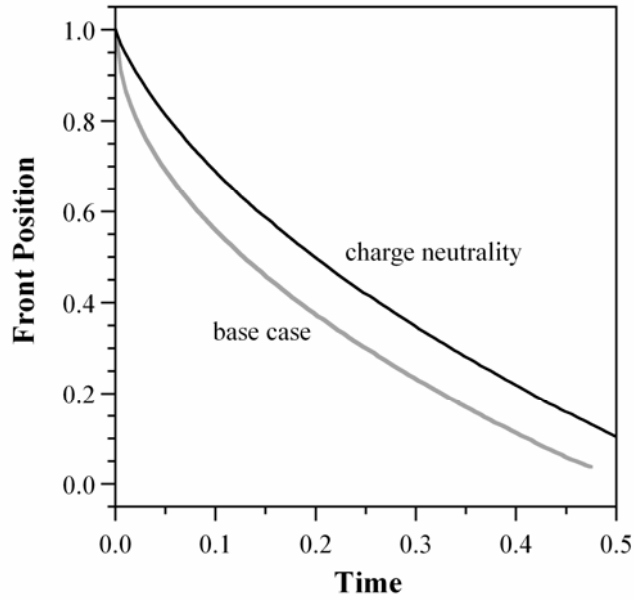
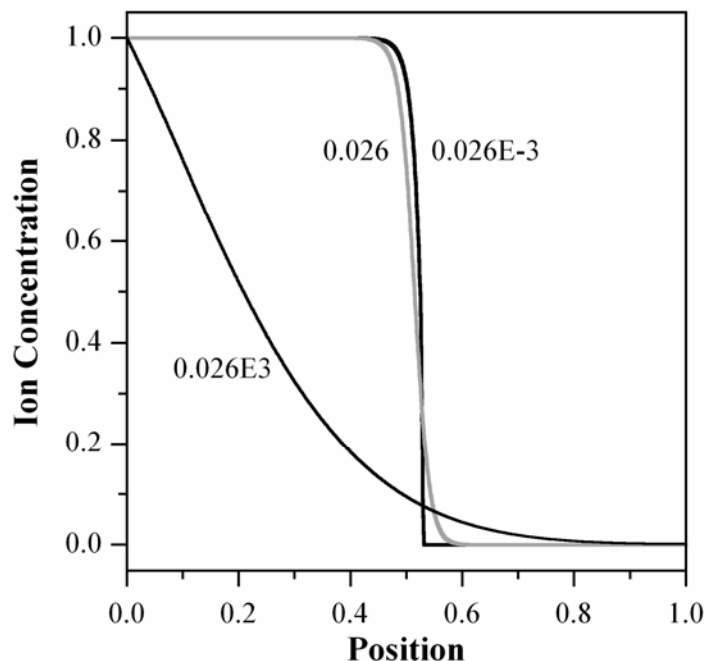


Figure SM 13. Front position vs. time for the charge neutral and base cases.

## 2.9 Effect of Varying $D/\mu$ (for section 4.3.2 Relationship Between $D$ and $\square$ )

We varied the ratio between diffusivity and mobility by 6 orders of magnitude. The resulting ion concentration profiles are shown in Figure SM 14. For  $D/\mu = 0.000026$ , the profile is similar to the ones at high voltage (compare Figure 9), showing the dominance of migration. The ion concentration profile with  $D/\mu = 26$  is bell-shaped, illustrating the dominance of diffusion.



**Figure SM 14. Ion concentration profiles for different  $D/\mu$  ratios. The ratio was raised (0.026E3) and lowered (0.026E-3) by three orders of magnitude from that in the Einstein relation (0.026, base case, shown by the gray line).**

These results show that by varying the relationship between diffusivity and mobility, ion concentration profiles can change from diffusion-like features to migration-like features. Increasing the ratio between diffusivity and mobility has an effect similar to lowering the reduction potential, while decreasing the ratio is similar to raising the potential. (Whether the Einstein relationship is valid for ions in conjugated polymers has not been established experimentally.)

### 3 Reduction in the Full Model

#### 3.1 Ion Flux in the Electrolyte (for section 5.2, Addition of the Electrolyte)

The section compares the drift and diffusion terms in the electrolyte to determine the importance of drift in the electrolyte. As shown in Figure SM 15a, the ions in the electrolyte move exclusively by drift between  $x = -10$  and  $-5$ , and increasingly by diffusion closer to the polymer interface, where there are substantial concentration gradients. Then, within 0.03 distance units of the polymer interface (Figure SM 15b), the migration component increases again, to large positive values, and the diffusion component goes to large negative values: the strong electric field pulls the cations toward the interface, but at the same time the high concentration of cations in the double-layer produces a large flux away from the interface back into the electrolyte. These two components approximately balance, the difference being the flux into the polymer.

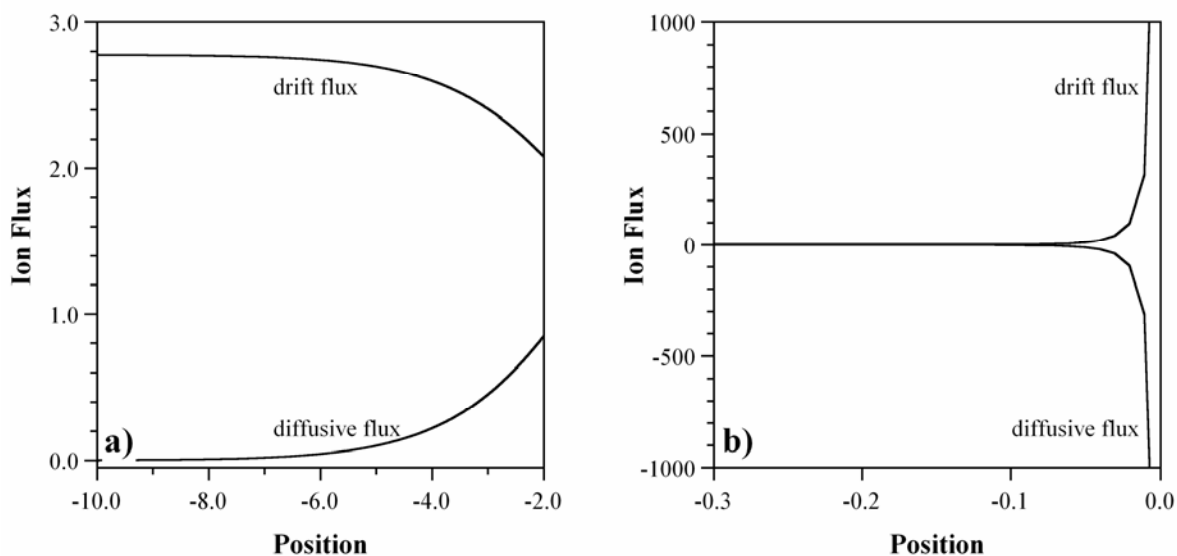


Figure SM 15. a) Diffusive and drift fluxes of cations in the electrolyte far from the polymer. B) Diffusive and drift fluxes in the double layer. Note the differences in scale from a).

### 3.2 Potential Drop over the Polymer (for section 5.2.2, Full Model Results)

Figure SM 16 shows the potential drop across the polymer over time in the full model, which includes the electrolyte. It increases rapidly until  $t = 0.01$  and then grows slowly until the film is fully reduced at  $t = 0.2$ .

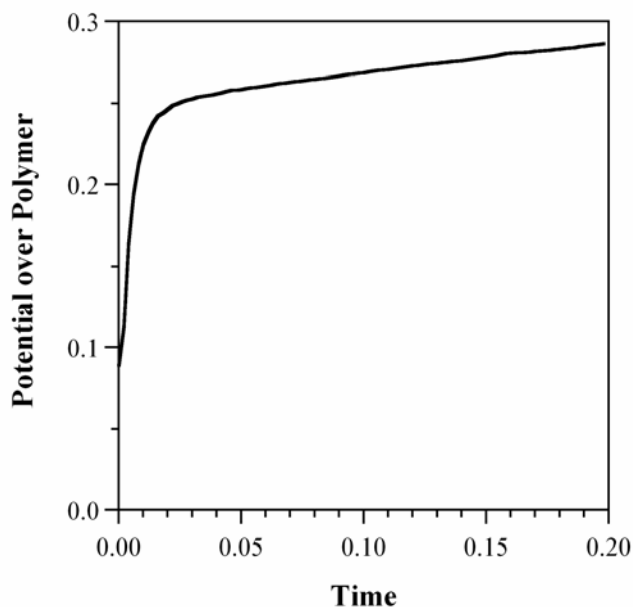
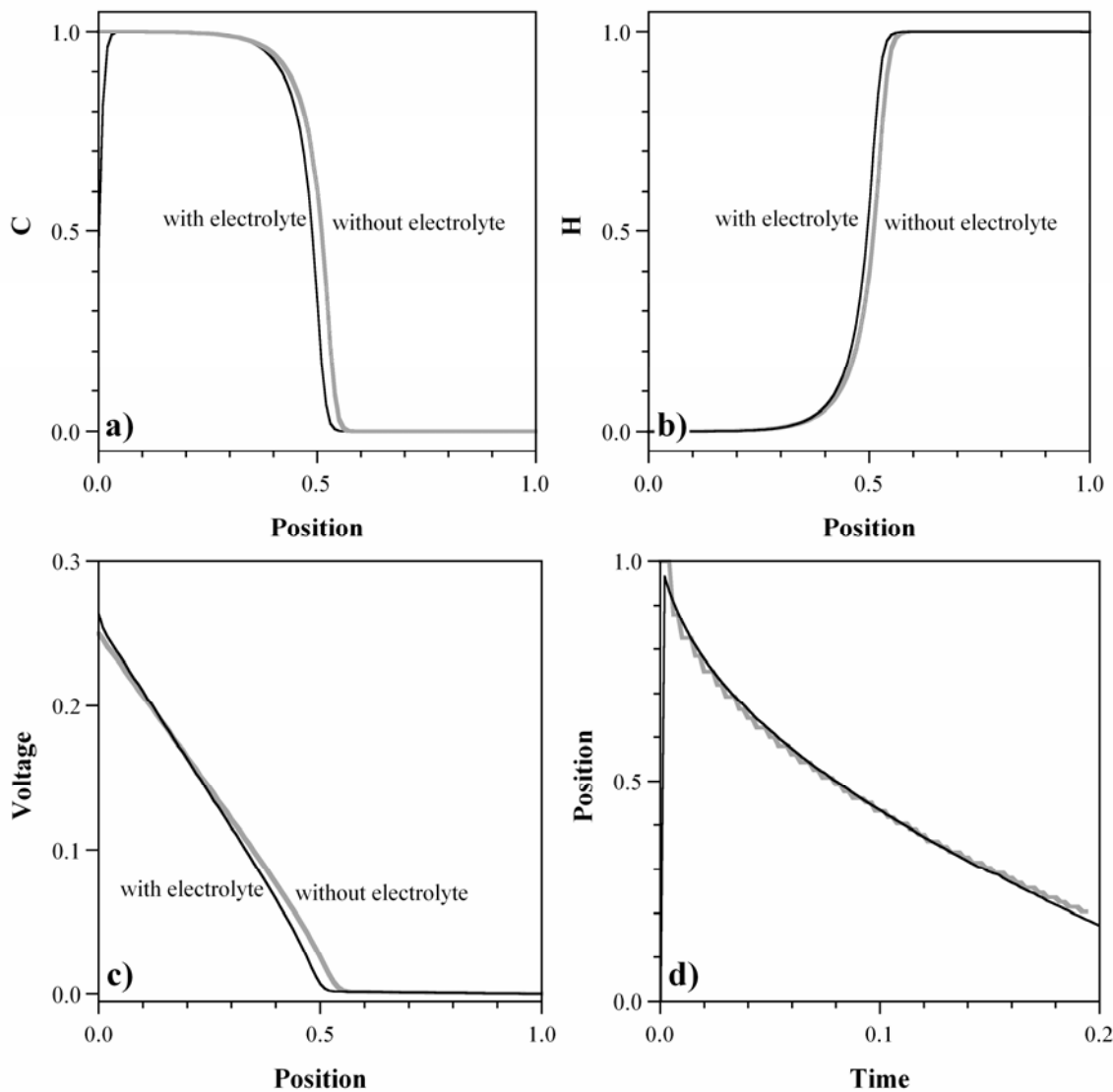


Figure SM 16. Potential drop over the polymer film over time in the full model ( $V = -1$ ); the rest of the voltage is dropped over the electrolyte.

### 3.3 Comparison between Full Model and Base Case (for section 5.2.2, Full Model Results)

Figure SM 17 shows the ion concentration profiles predicted by the models in sections 5.1 and 5.2 at the same time ( $t = 0.08$ ) when  $V = 0.25$  is applied in the former, and  $V = 1$  in the latter. The only difference is that the base case profile is slightly ahead of that in the full model. This is because the ion concentration at the polymer/electrolyte interface in the full model is smaller

than  $C_{max} (= 1)$ . The two models thus behave the same way when the potentials across the polymer are the same.



**Figure SM 17. Results at  $t = 0.08$  from the full model with an applied potential of  $V = 1.0$  (black) and the base case model with an applied potential of  $V = 0.25$  (gray). a) Ion concentration, b) hole concentration, c) potential, and d) front position.**

### 3.4 Full Model with Diffusion Only (for section 5.2.3, Variation: Diffusion Only)

In the paper, we showed the result of neglecting cation migration in the polymer. Here we present four additional simulations in which the full model is driven by diffusion only. In the first, we examine how the addition of a capping function changes the results presented in the main text. In the second, the cation mobility in the polymer is set to zero and the diffusivity is given a stronger dependence on ion concentration. In the third, both ions and holes in the polymer are driven by diffusion only. In the last case, the ions in the electrolyte are driven by diffusion only.

#### 3.4.1 Diffusion-Based Capping Function

The case presented in the paper could not employ a migration-based capping function for the charge, since the migration term was already set to zero everywhere. This section instead uses a capping function based on diffusion:

$$(28) \quad D_C = D_0(1 + 0.01e^{15(C - 0.8)}).$$

Figure SM 18 compares the ion concentration profiles for diffusion-only in the polymer with (black) and without (gray) capping. The only difference is that in the latter case, the profiles are slightly more advanced, but the effect is small because the ion concentration in the film never goes that high. For example, at  $t = 0.02$ , the ion concentration at the interface is only 1.15, resulting in a diffusivity increase of 2.9 there.

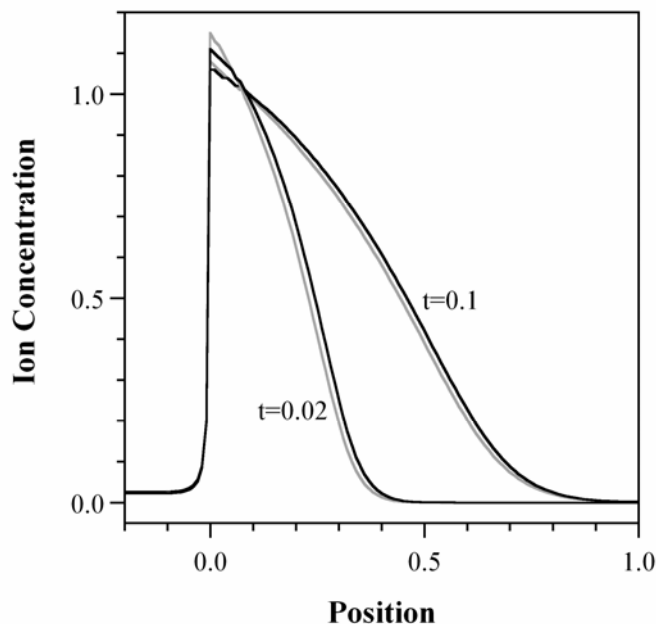


**Figure SM 18. Ion concentration profiles (black lines) when migration in the polymer is turned off and the capping function in equation (28) is applied. The gray lines show the profiles without capping.**

### 3.4.2 Ion Diffusivity Proportional to $e^{5C}$

This section examines how the simulation results are affected when a steeper relationship between diffusivity and ion concentration is used:  $e^{2C}$  is replaced by  $e^{5C}$ . At low potentials ( $< 1$ ), the maximum ion concentration was always lower than 1 (Figure SM 19a), even after long times. At high potentials (Figure SM 19b),  $C$  reached  $C_{max}$ , although it exceeded  $C_{max}$  at early times. The final ion concentration is shown as a function of voltage in Figure SM 19c. When the reduction voltage is increased, the front velocity increases logarithmically (Figure SM 19d), which is inconsistent with the experimental results. The front velocity increases because higher voltages lead to higher ion concentrations at the interface.

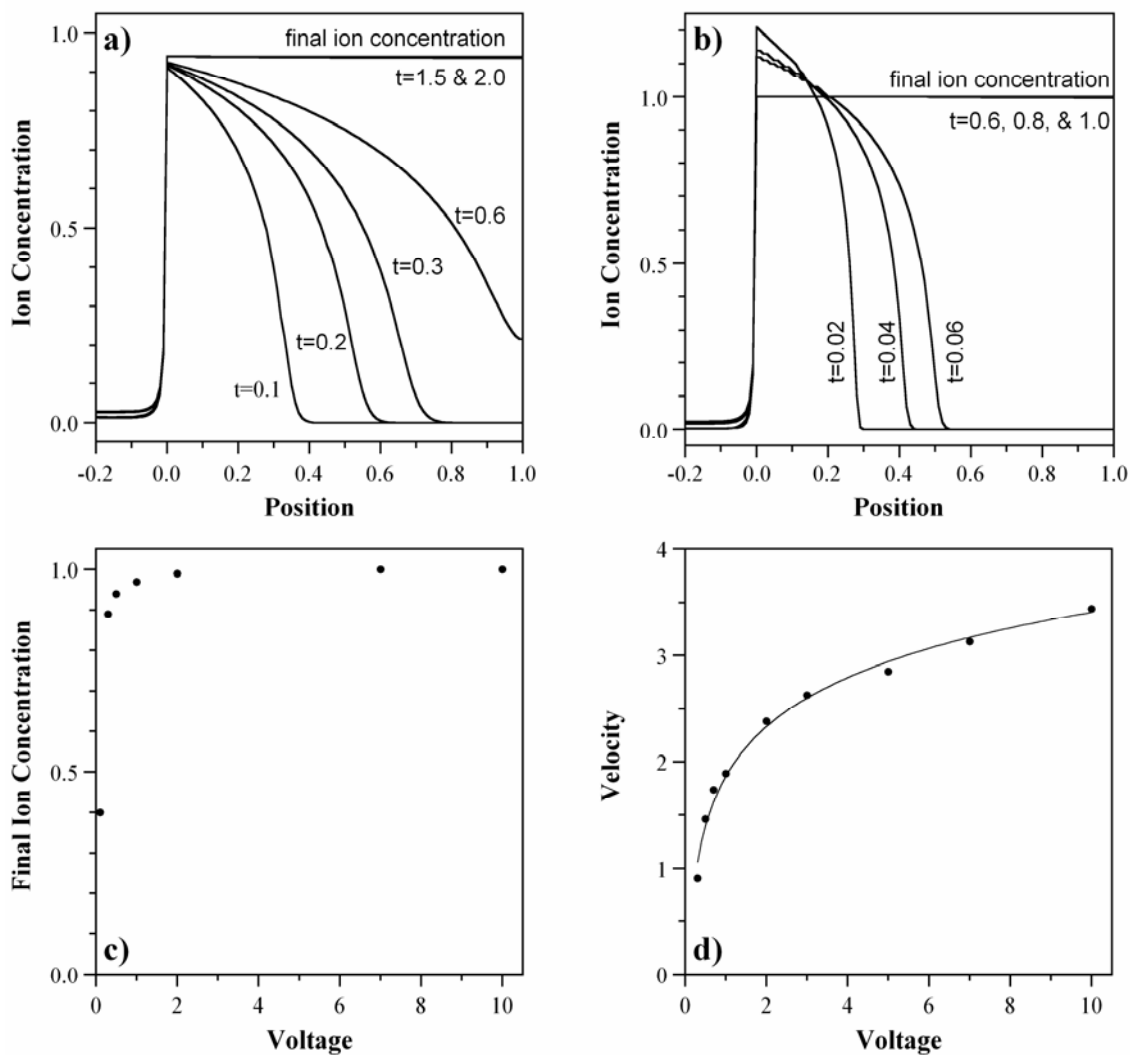


**Figure SM 19. Ion concentrations and front velocities during reduction when ion migration is turned off in the polymer and  $D_C = D_0 e^{5C}$ . Concentration profiles for a)  $V = 0.5$  and b)  $V = 7$ . c) Final ion concentrations in the polymer at the end of the reduction process for different applied potentials. d) Front velocity vs. potential. The line shows a log fit.**

### 3.4.3 Ions and Holes in the Polymer Driven by Diffusion Only

In the previous cases, the *holes* in the polymer were still moving by migration. Figure SM 20 shows the potentials in the polymer at two different times when migration is set to zero for both

ions and holes. The potential is dropped only over the polymer. Since the potential drop in the electrolyte is small, no double layer is formed at the interface (Figure SM 21). Ions enter the polymer at a very low rate and cannot reach  $C_{max}$ . Even at long times ( $t = 50$ ),  $C$  only reaches 0.1, and the film is far from fully reduced.

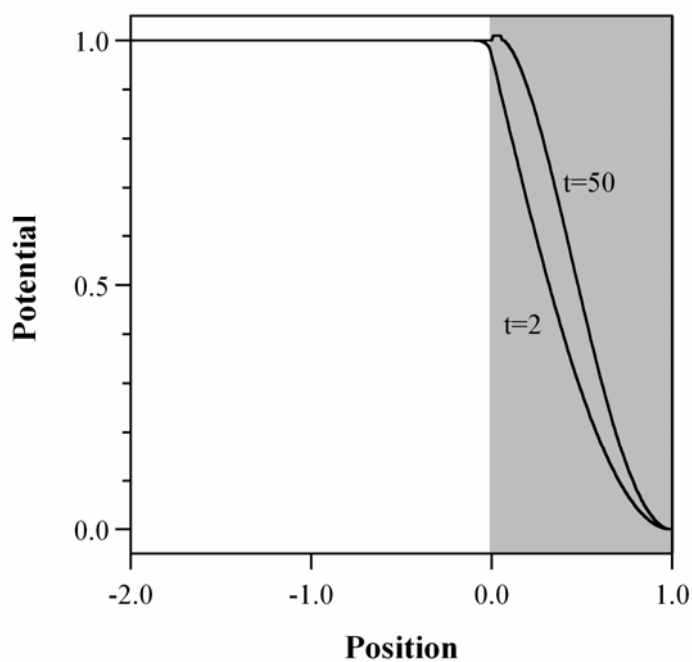


**Figure SM 20. Potential profiles when ions and holes in the polymer are driven only by diffusion.**

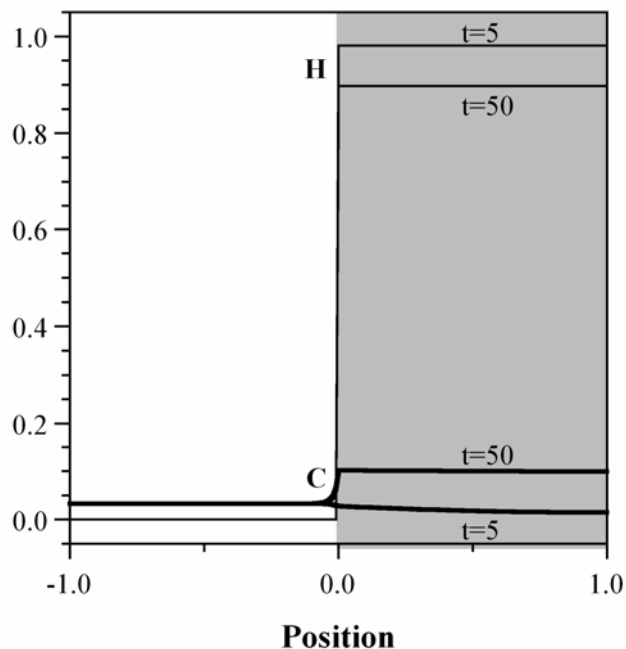


**Figure SM 21. Ion and hole concentrations when ions and holes in the polymer are driven only by diffusion.**

#### 3.4.4 Ions in the Electrolyte Driven by Diffusion Only

This section examines the effect of turning off migration in the electrolyte (preventing the transport of ions by migration to the electrolyte/polymer boundary), but leaving migration *on* in the polymer. Figure SM 22 shows that under these conditions, the ion concentration in the polymer remains equal to the bulk electrolyte concentration no matter how long the simulation runs, and the film cannot be reduced.

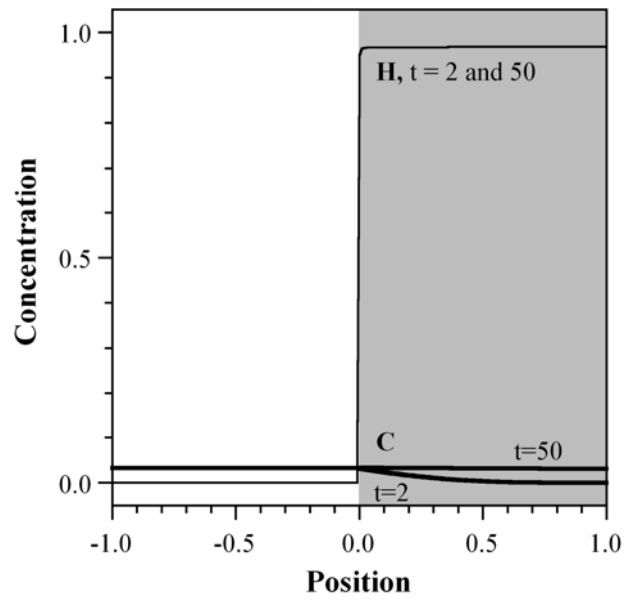


**Figure SM 22. Ion and hole concentrations when ions in the electrolyte are driven only by diffusion.**